Aalto-yliopisto
Insinööritieteiden
korkeakoulu

Ilkka Ekström

DEVELOPMENT OF INJECTOR NOZZLE SECTIONING

Thesis submitted as a partial fulfillment of the requirements
for the degree of Master of Science in Technology
Södertälje, Sweden 4.4.2016
Supervisor: Professor Kalevi Ekman
Instructor: M.Sc. Sara Alfredsson

Aalto-yliopisto
Insinööritieteiden korkeakoulu

Diplomityön tiivistelmä

Tekijä Ilkka Ekström

Työn nimi Ruiskutussuuttimen poikkileikkausmenetelmän kehitys

Koulutusohjelma Konetekniikka

Pää-aine Koneensuunnittelu **Koodi** K3001

Työn valvoja prof. Kalevi Ekman

Työn ohjaaja DI Sara Alfredsson

Päivämäärä 04.04.2016 **Sivumäärä** 57+4 **Kieli** englanti

Tiivistelmä

Kasvava tietoisuus käynnissä olevasta ilmastonmuutoksesta on saanut valtiot ja viranomaiset ryhtymään toimenpiteisiin, että hiilijalanjälkeä saataisiin pienemmäksi. Tämä on johtanut useiden erityyppisten biopolttoaineiden kehitykseen. Autoteollisuuden ja loppukäyttäjien kiristyvät vaatimukset nostavat puristussytytysmoottoreiden suorituskykyvaatimuksia, mikä on lisännyt polttoainetaloudellisemman ja vähäpäästöisemmän tekniikan kysyntää.

Autovalmistajat ympäri maapalloa ovat havainneet, että nykyisten moottorien ominaisuudet aiheuttavat ruiskutussuuttimien pinnoille sakkautumia. Sakkautumilla voi olla negatiivinen vaikutus moottorin suorituskykyyn, johtaen esimerkiksi lisääntyneeseen polttoaineenkulutukseen ja kasvaneisiin päästöihin. Jatkuvan biopolttoaineiden ja moottorien ominaisuuksien kehittämisen seurauksena uudentyyppisten sakkautumien esiintyminen on odotettua.

Tämä diplomityö on osa Scanian ja KTH:n välistä yhteistyöprojektia, jonka tavoitteena on tutkia tulevaisuuden polttoaineenruiskutusjärjestelmien kestävyyttä. Projektin tavoite on tarkastella mahdollisia eri polttoainelaatujen aiheuttamia heikkouksia tulevaisuuden ruiskutusjärjestelmissä sekä tutkia eri polttoaineparametrien vaikutusta sakkautumien syntyyn ja poistoon. Erityisen kiinnostuksen kohteena ovat sakkautumat, jotka muodostuvat suuttimien suihkutusreikien sisäpinnoille. Jotta näiden sakkautumien tutkiminen mikroskoopilla olisi mahdollista, tarvitaan poikkileikkausmenetelmä, joka ei prosessin aikana vahingoita tai poista niitä. Tällä hetkellä käytössä oleva menetelmä ei ole tarpeeksi luotettava ja toistettava, sillä tuloksena saatujen poikkileikkausten muoto ja näkyville saatujen reikien seinämien määrä ovat epäjohdonmukaisia.

Tässä diplomityössä esitellään potentiaaliset menetelmät poikkileikkauksen tekemiseen. Menetelmät on jaettu koneistus- ja rikkomismenetelmiin. Tämän lisäksi esitellään yksi rikkomaton menetelmä. Parhaat menetelmät valitaan sopivuuden ja saatavuuden perusteella testattavaksi. Testit ja testitulokset esitellään jokaisesta menetelmästä, minkä jälkeen esitetään tulosten perusteella tehdyt johtopäätökset.

Lopputuloksena kehitetään toistettava ja luotettava leikkausmenetelmä, jota tullaan tulevaisuudessa käyttämään ruiskutussuuttimien suihkutusreikien sisäpinnoille muodostuneiden polttoainesakkautumien tutkimisessa.

Avainsanat ruiskutussuutin, polttoainesakkautumat, poikkileikkaus, menetelmän kehitys, ruiskutusjärjestelmä, puristussytytys

Aalto-yliopisto
Insinööritieteiden
korkeakoulu

Abstract of master's thesis

Author Ilkka Ekström

Title of thesis Development of injector nozzle sectioning

Degree programme Mechanical Engineering

Major Machine Design **Code** K3001

Thesis supervisor Prof. Kalevi Ekman

Thesis advisor M.Sc. Sara Alfredsson

Date 04.04.2016 **Number of pages** 57+4 **Language** English

Abstract

With increasing awareness of the ongoing climate change, governments and authorities around the world have begun to take actions to reduce the carbon foot print. It has led to an increased development and usage of various biofuels. Tightening regulations in automotive industry and requirements of the end users are increasing the performance requirements on compression ignition engines, leading to a need for better fuel economy and lower emissions.

Automotive manufacturers around the globe have observed that the current engine features are causing injector nozzle deposits. The deposits can have a negative impact on engine performance, resulting for example in increased fuel consumption and emissions. Due to continuous development of biofuels and engine characteristics, new types of injector nozzle deposits are expected in the future.

This thesis is part of a cooperation research project between Scania and KTH, in which future fuel injection system robustness against soft particles is studied. The objective of the project is to examine weaknesses in future injection systems with different fuel qualities and study the effect of different fuel parameters on deposit build-up and removal.

Special areas of interest in the project are the deposits building up inside the nozzle spray-holes. In order to study the deposits with a microscope, a sectioning method, which doesn't contaminate or remove the deposits, has to be developed. Problems with the current used method are the inconsistency of the obtained cross-sections and the lack of exposed spray-holes.

In this thesis, potential methods for injector nozzle sectioning are introduced. The methods are divided into machining and destructive methods. In addition, one potential non-destructive method is introduced. Based on the suitability and the availability, the best methods are selected for further testing. The test methods and results are presented for each method, after which conclusions are made and the best method is recommended.

As a result of this thesis, a repeatable and reliable drop-weight method is developed. The method will be used in the future for studying of internal fuel deposits that are built up in the nozzle spray-holes.

Keywords injector nozzle, fuel deposits, sectioning, method development, fuel injection system , compression ignition

Acknowledgements

This thesis was written between October 2015 and March 2016 at Scania CV AB in Södertälje, Sweden.

I would like to thank my instructor M.Sc. Sara Alfredsson for giving me this interesting opportunity and for supporting me throughout the process with dedication and enthusiasm. I would also like to thank the supervisor of this thesis, Professor Kalevi Ekman, for guidance and support. Thanks to the whole Scania UTMB department for the great working atmosphere and the support along the way.

Special thanks go to my parents for supporting me during my studies and for encouraging me to go forward in life. Thanks to my girlfriend Anna who has always believed in me and told me to challenge myself time after time.

Södertälje, Sweden
Monday, 4 April 2016

Ilkka Ekström

Table of contents

List of symbols

A	Area
D	Outer diameter of a cylinder
D_i	Internal diameter of a cylinder
F	Force
$K'_{xx}, K'_{yy}, K'_{xy}$	Stress concentration factors
P	Applied load
T_1	External surface boundary of a ring-disc
T_2	Internal surface boundary of a ring-disc
W	Work
W_y	Force applied in y-direction
W_f	Load applied when a specimen fails
d	Traveling distance after impact
g	Gravitational acceleration
h	Height
m	Mass
t	Length of a cylinder
v	Velocity
α	Loading angle
ρ	Ratio between internal and external diameter of a cylinder
σ	Tensile stress

List of abbreviations

3D	Three-Dimensional
BIB	Broad Ion Beam
CAD	Computer Aided Design
CBN	Cubic Boron Nitride
CBN-U	Cubic Boron Nitride Ultrafine-crystalline
CNC	Computer Numerical Control
EBM	Electron Beam Machining
FIB	Focused Ion Beam
HAZ	Heat-Affected Zone
KE	Kinetic Energy
KTH	Kungliga Tekniska Högskolan
LASER	Light Amplification by Stimulated Emission of Radiation
LOM	Light Optical Microscope
PE	Potential Energy
SEM	Scanning Electron Microscope
cw	continous wave
fs	femtosecond
ns	nanosecond
ps	picosecond

1 Introduction

With increasing awareness of the ongoing climate change, governments and authorities around the world have begun to take actions to reduce the carbon foot print. This has led to an increased development and usage of different biofuels. The market nowadays consists of fuels with varying properties and qualities. Tightening regulations in automotive industry and requirements of the end users are increasing the performance requirements on compression ignition engines, leading to a need for better fuel economy and lower emissions. These challenges have been partly solved by improving the injection equipment and combustion conditions, which has led to multiple injections, higher injection pressures and increased operating temperatures. (1)

Automotive manufacturers around the globe have observed that these current circumstances are causing growing amounts of injector nozzle deposits, which can occur for example inside the injector body or spray-holes of the nozzle tip. Problem with the deposits is that they can have a negative impact on engine performance. Formation of deposits can cause increased fuel consumption, loss of power and increased emissions. (2) With constantly developing biofuels and engine features, new types of deposits are expected. To have deeper understanding about the formation, causes and effects of these new types of deposits, they need to be studied.

This thesis is part of a cooperation research project between Scania and KTH, in which future fuel injection system robustness against soft particles is studied. Scania is developing its own fuel injection systems in collaboration with Cummins Fuel Systems. The objective of the project is to examine weaknesses in future injection systems with different fuel qualities and study the effect of different fuel parameters on deposit build-up and removal. In order to study the injector nozzle deposits, the nozzles need to be opened up. Special areas of interest in the project are the deposits inside the nozzle spray-holes.

The current method that Scania has developed includes liquid nitrogen and mechanical force. Firstly, the nozzle is dipped into a liquid nitrogen bath to make the material more brittle. Then the nozzle is crushed by squeezing it in a mechanical press. The problem is that the effect of liquid nitrogen to the deposits has not been studied, and the manual crushing doesn't give repeatable results. The manual crushing results in inconsistent cross-sections where only some of the nozzle holes are exposed. In addition, the few holes that are exposed, give frequently only a partial visible access inside the walls of the holes.

2 Objective

The objective of this master's thesis is to develop reliable and accurate methods to section diesel injector nozzles without contaminating, damaging or removing the deposits.

First target is to identify as many suitable methods as possible and choose the most potential ones for further examination. Second target is to study and test the suitability of the chosen methods in practice. Final target of the thesis is to develop a reliable and repeatable process for injector nozzle sectioning.

3 Included nozzle types

Different injector nozzle types included in the project were defined in order to help the identification of potential methods. The nozzle types are called type A and type B.

All of the nozzle types are machined from AISI H13 tool steel and then gas-nitrided. The nozzle spray-holes are machined afterwards, which means the internal surfaces of the holes do not have a nitride coating. Diameter of the spray-holes is approximately 0.1 mm and the depth of a single hole is around 1.15 mm depending on its location in the tip.

4 Desired cross-section

The desired cross-section is shown in Figure 1. The objective is to reveal all the holes from the whole length. This can be achieved by creating a cross-section which has basically a conical shape. A conical shape has to be sectioned, because the holes are not perpendicular to the longitudinal central axis of the nozzle. It means that, for example if a cutting method would be used, the process has to be carried out in an angle which is parallel to the angle of the holes.

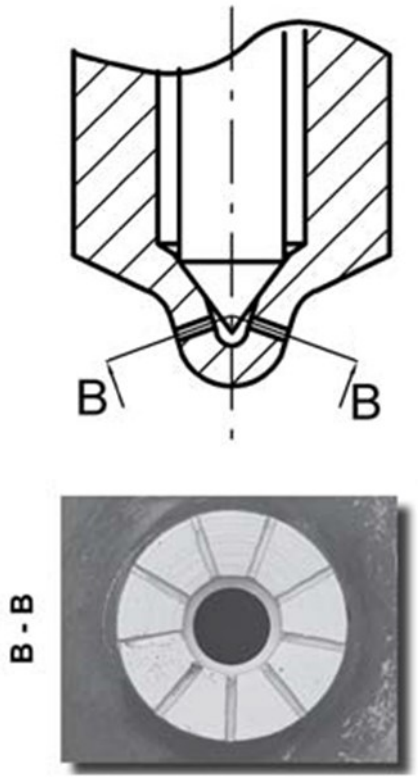

Figure 1. The desired conical tip cross-section. (3)

5 Literature review

The literature review was made with the requirements of this application in mind. The defined requirements for a suitable method are listed below:

- applicable for metals
- high precision
- material removal in micro-scale
- minimal risk of deposit contamination
- minimal risk of deposit removal.

The possible methods for injector nozzle sectioning are divided into machining methods and destructive methods. In addition, one non-destructive method is introduced.

5.1 Machining methods

Since the risk of deposit removal and contamination had to be minimal, methods like water-jet cutting and electro discharge machining were left out from this literature review due to the presence of liquid jet and liquid bath.

5.1.1 Laser beam machining

The word laser comes from light amplification by stimulated emission of radiation (4) (5) (6). Laser is a source of coherent and amplified beam of electromagnetic radiation. The difference between a laser and an ordinary light source is the emission process of radiation. In an ordinary light source, photons are emitted spontaneously in a random manner because the atoms or molecules are excited thermally for example by electrical discharge. In lasers instead, stimulated emission is used for emitting the photons, which leads to photons having the same frequency, wavelength and phase. In other words, photons get amplified in an orderly manner. This is why laser beams are highly directional, have high power density and better focusing characteristics. These characteristics can be used in processing of different materials. (5) (6)

Laser beam cutting is one of the most used industrial application of lasers in metal industry, which enables cutting of almost all materials that are known (5) (7). Laser cutting is a desirable technology in comparison with other conventional or non-conventional cutting methods because it provides high material versatility, edge quality, accuracy, production flexibility and material utilization. (7)

Laser cutting has several advantages when compared to other cutting processes such as oxy-fuel cutting or plasma cutting. Those advantages include a narrow cut with minimal area subjected to thermal effects, a proper cut profile, smooth and flat edges, minimal deformation, high cutting speeds and fast adaptation to manufacturing program changes. (5) Figure 2 illustrates the principle of laser cutting process.

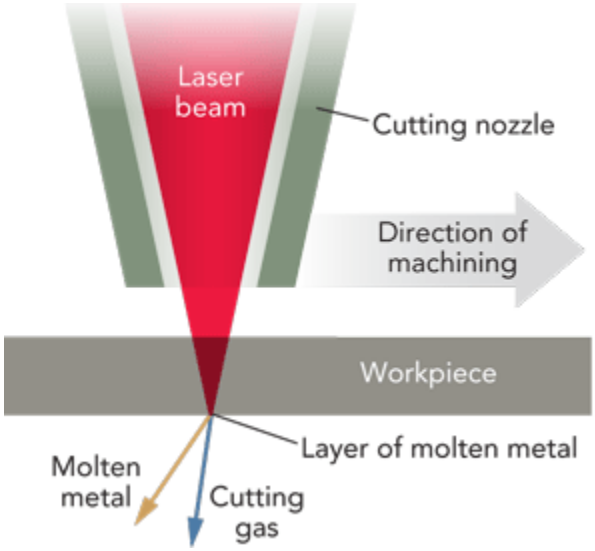

Figure 2. Principle of laser cutting process. (8)

Pulsed laser cutting

Lasers for micro-processing, such as micro-cutting, are used to cut more complex and smaller shapes (9). Lasers can be divided into continuous wave (cw) lasers and pulsed lasers. Pulsed lasers are a better solution for processing of micro-sized structures because of the much higher intensity they can achieve when compared to continuous wave lasers. Pulsed lasers are divided into long-pulsed (nanosecond, ns), short-pulsed (picosecond, ps) and ultrashort-pulsed (femtosecond, fs) lasers. Because of material vaporization through high peak powers and extremely short interaction times, pulsed lasers produce a small heat-affected zone (HAZ) and a small recast layer on the workpiece compared to continuous wave lasers. Using of short-pulsed and ultrashort-pulsed lasers enables extremely localized heating on the micro-scale, which leads to even more reduced thermal damages in the workpiece (Figure 3). Thermal damages are often harmful and a limiting factor in applications where high precision is needed. (10)

Pulse duration has an important effect on laser machining. When pulse duration is kept short, it maximizes peak power and minimizes thermal diffusion to the surrounding material, which leads to very localized heating. (10) It has been studied, that pulse duration between 5 to 10 picoseconds appears to be optimal for micro-machining of metals (11).

Ultrashort-pulsed lasers are very promising for the future applications in precision machining. Laser cutting is still a thermal process which means that for example HAZ, recast layer or chemical contamination cannot be fully avoided. (10)

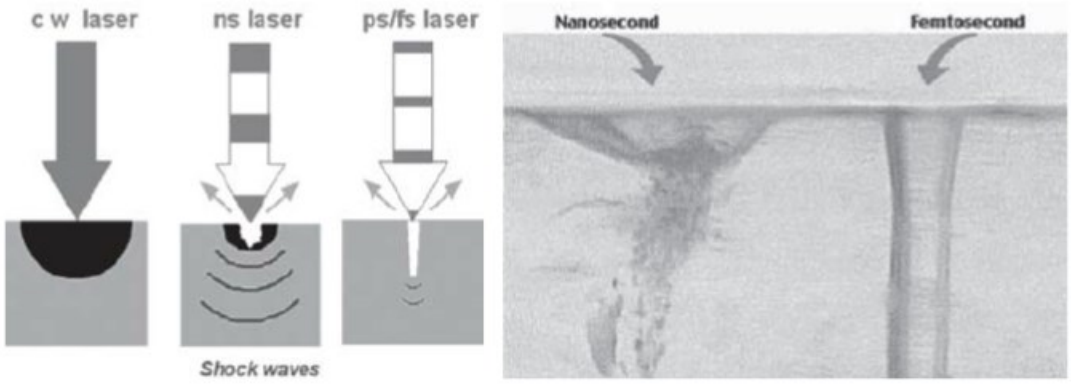

Figure 3. Comparison of thermal effects, shock waves and groove width between different laser types. (10)

Helical laser cutting

In the ultrashort-pulsed laser technology, a method with increased efficiency and accuracy has been reported (11) (12). The so-called helical drilling method, in which the laser ablation front penetrates the workpiece on a helical path, has been proved to be a more competitive micro-machining method with precise and flexible controllability on the geometry and morphology of holes and cutting grooves. Based on the principles of helical laser drilling, a precise cutting technique called helical cutting has been developed. (12)

The high-speed rotation in helical radius enables an easy formation of cylindrical, positive or negative conical cutting grooves. Another advantage of the helical laser movement is, that the surface quality in the cutting groove is improved. Because of the helical motion of the laser beam, the width of the cutting groove is basically larger and the cutting speed is lower compared to conventional cutting methods. But on the other hand debris and striation formation can be avoided and the cutting quality is clearly improved. (12)

The double-pulse effect

In long-pulsed laser machining, a ”double-pulse” effect has been observed. It has been studied that when two nanosecond laser pulses are separated by a delay time of 30–150 nanoseconds, the ablation rate per pulse and the machining quality are considerably increased compared to the conventional pulsed laser ablation, where pulses are separated by at least 100 microseconds (10). Figure 4 shows the difference in results between conventional laser drilling and double-pulsed laser drilling.

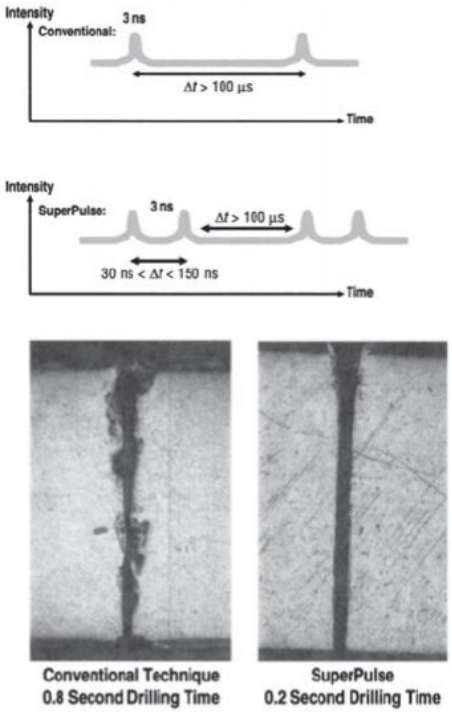

Figure 4. The difference between conventional laser drilling and double-pulsed (SuperPulse) laser drilling. (10)

Suggestion for the reason behind this effect is, that the first laser pulse ablates the surface and generates a plasma cloud with high temperature. The second pulse does not hit the surface of the material but instead it interacts with the plasma cloud and raises the temperature and velocity of the ablated material in the cloud which is lingering above the surface. It has been proposed that this energetic plasma enhances rapid fresh material ablation and prevents re-deposition of the ablated material. (10)

5.1.2 Plasma arc machining

Plasma is highly heated ionized gas and it is usually described as the fourth state of matter (13). Plasma arc cutting is a thermal process which uses a constricted jet of high-temperature plasma gas to melt and separate metals (14) (15) (16). The formation of plasma arc happens inside a water cooled torch and is struck between a negative electrode and a workpiece (Figure 5). The energy from the arc ionizes a portion of the gas and brings it to the plasma state. The geometry inside the plasma torch forces the mixture of heated gas and plasma to flow through a narrow hole where it is superheated due to ohmic heating. Outside the torch, a supersonic jet strikes to the working surface and is assisted with a shielding gas. Shielding gas covers the cutting zone, helps in cooling the torch and constricting the plasma jet. (15) (17)

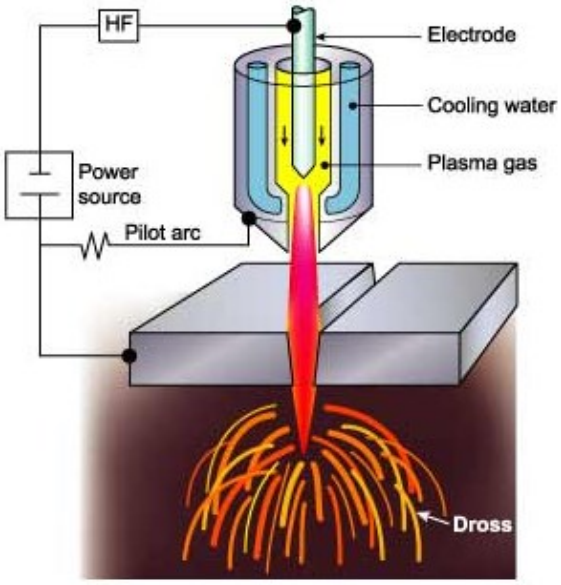

Figure 5. The principle of plasma arc cutting. (18)

Plasma arc cutting can be used for cutting variety of electrically conducting materials such as stainless steel, manganese steel, titanium alloys, copper, magnesium, aluminum alloys and cast iron. (17) (19) The most commonly used gases for plasma cutting are air, argon, nitrogen and hydrogen. (16) (19)

Compared to laser cutting, plasma cutting is not as precise and the heat affected zone caused by a plasma cutter is relatively larger (16) (20). Plasma cutting machines are much cheaper than laser cutting machines, but lose on process flexibility and automation capabilities to laser (20) (21). Plasma cutting torches, which constrict the arc to produce narrow kerfs and high arc density, have been developed for micro-cutting. These micro-nozzles enable the production of high precision cuts at lower cost than laser. The disadvantage is that the micro-nozzle technology does not provide as high quality and precision as lasers. (22)

5.1.3 Ion beam machining

An ion beam is a beam of highly energetic ions which can be manipulated electrically. Material removal with ion beam is carried out by knocking atoms out of the working surface. Electro-elastic collision and recoil action between the ion and the target surface results in ion sputtering. The stream of charged ions is accelerated in a vacuum and then directed towards the workpiece. (23)

Broad Ion Beam and Focused Ion Beam

Broad Ion Beam (BIB) and Focused Ion Beam (FIB) are advanced complementary methods for preparing precise cross-section surfaces for a wide variety of different materials. Difference between the two methods is that FIB provides higher removal rates, but the effective area that can be revealed per time unit is very limited (~10 µm*10 µm). BIB instead provides lower removal rates, but the effective area that can be revealed per time unit is relatively larger (~1 mm*1 mm). (24) (25) Another difference is the used ion source. Argon is used in BIB and in FIB a gallium liquid metal ion source is the most commonly used source of ions. (25) (26)

FIB is a focused beam of positive ions, which has a diameter from a few nanometers to a few micrometers. FIB-milling is used today for preparation of cross-sectional samples for electron microscopes. (27)

Due to the short wavelength and large energy density, FIB is able to fabricate structures that have feature sizes below 1 µm. (28) Gallium liquid metal ion is the most commonly used source due to its reliability, reproducibility, stability and lifetimes beyond 1000 hours. Gallium is also capable of providing a beam size of ~5 nm. (29) FIB milling enables site-specific milling with high positional accuracy. It is a non-thermal method which means stress-free milling without any thermal effects to the workpiece. There are no other techniques to cut thin samples stress-free with such a high accuracy. (27) FIB has reportedly been used for cutting thin sample slices from diesel injector nozzles (3).

Plasma Focused Ion Beam

Plasma FIB system has a xenon plasma ion source instead of a conventional liquid gallium ion source (30) (31). Typically, milling rates of 50 times faster than with the gallium ion beam, have been reported. Therefore it is possible to mill volumes that could not be achievable in reasonable time with a conventional FIB. (30) (31) (32) The high milling rates of the developed plasma FIB enables it to be used in rapid fabrication of such devices as mechanical micro-tools, micro coils, microfluidic channels and nozzles. Plasma ion beams can be focused to spot sizes in the range of 2–30 µm. (32)

As an example, milling of 400 µm*100 µm*500 µm cross-section through silicon (Figure 6) has been reportedly milled in 45 minutes. With a conventional gallium source FIB the process would have taken more than one day. (33)

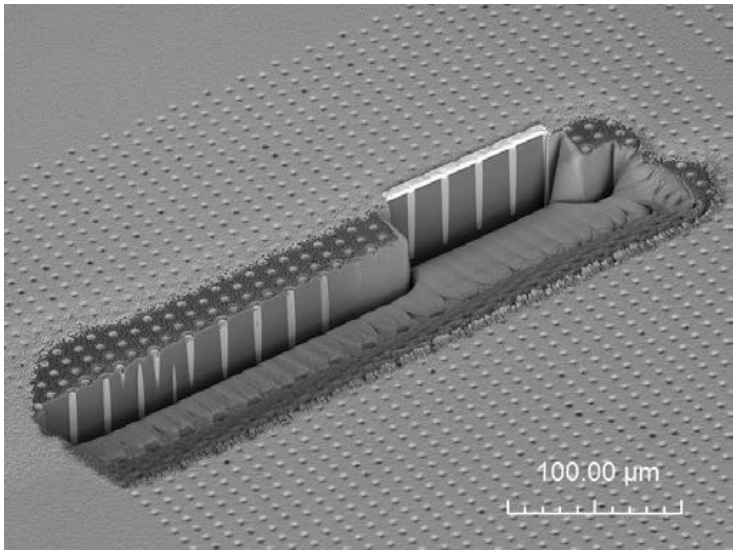

Figure 6. Cross-section made through silicon with Plasma FIB. (33)

5.1.4 Electron beam machining

Electron beam machining (EBM) is a thermal machining process, which is used for heating, melting or vaporizing of different materials. The principle of EBM is that electrons with a high velocity are concentrated into a narrow beam. When the high-speed electrons in a focused beam impact the material surface, most of their kinetic energy converts into heat energy. The beam is focused and deflected by electromagnetic lenses and the power density is controlled by modifying the acceleration voltage. (34)

EBM requires a vacuum operating chamber, because otherwise the electrons would interact with the air molecules and lose their energy. In the operating chamber, the workpiece is fixed to an operating table and it can be moved to x or y direction under the beam. The spot size and focal length are controlled by a current flowing through a coil, through which the beam is guided. An electron beam which has a diameter of less than 1 µm can be obtained. The process is used for many applications such as drilling, cutting, annealing and welding. Materials like steel, stainless steel, aluminum, plastics and ceramics can be machined by using EBM. (34) (35) Figure 7 illustrates the fundamentals of EBM.

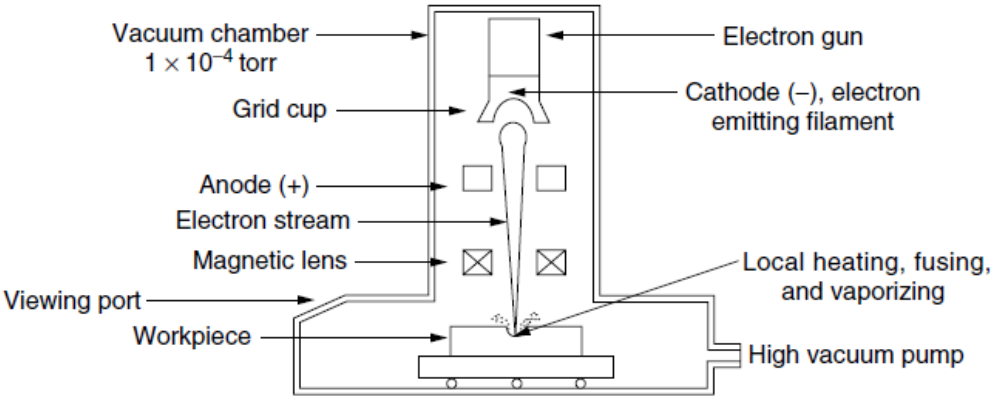

Figure 7. Fundamentals of EBM. (35)

The feature of the electron beam gives EBM certain advantages. The beam can be electromagnetically focused to even nanometer level with low current condition. An electron can be accelerated to extremely high velocity, which means that very high power densities can be obtained. With EBM, the material removal effectively progresses along the depth direction pulse by pulse and a deep keyhole can be created inside the workpiece. Therefore, deep penetration is possible. Short pulse oscillation of the beam is possible, and when it is synchronized with the deflection, drilling of large number of micro holes can be done with high speed and accuracy. (34) Disadvantages of the method are the need for auxiliary backing material for the workpiece, high equipment costs and the need for a vacuum chamber (35).

5.1.5 Mechanical milling

In mechanical milling a machine tool removes metal from the workpiece with a rotating multipoint cutter (Figure 8). With the help of multiple cutting edges and rotation at high speed, the milling cutter removes metal at a very fast rate. (36)

Figure 8. Mechanical milling with 5-axis CNC milling machine. (37)

The capability of micro-mechanical machining and particularly micro-milling in manufacturing of a wide range of different materials and complex three-dimensional shapes makes it one of the best options to manufacture micro-parts. A miniature cutting tool is used to remove material from various engineering materials, including steel. (38) Micro-milling enables the creation of parts with dimensions of 1 μm (39).

The disadvantages of the method are low productivity and tool wear (38) (40) (41). Micro-cutting tools have low flexural stiffness and strength. Due to the fragile nature of cutting tools, the feed rates are small, leading to increased machining times. To compensate the machining time, high-speed machines are required in micro-milling process. (38) Increase in spindle speed decreases the cutting forces and tool deflection, which means that deformations in mill and controller structures become more ruling. Micro-mills are small and flexible, which makes vibrations of the machine a major problem. The process requires high precision and even small vibrations in the controller dynamics are harmful. (39) Due to the small size of the cutting tools, tool wear and breakage are hard to monitor (38) (40).

Majority of the milling tools are coated to reduce friction and heat generation at working interfaces (38) (41). Micro-milling tools can have a diameter as small as 5 μm (42).

5.1.6 Mechanical grinding

Grinding is a material removal method which is used for shaping and finishing components that are made of metals and other materials. An abrasive product, usually a rotating wheel is usually used to create a controlled contact with the workpiece. Grinding wheels consist of abrasive grains which act as a cutting tool by removing tiny chips of material from the workpiece. (43)

Micro-grinding enables the manufacturing of micro components and microstructures in various materials.

The method is used when the part accuracy demands are in the region of 1–5 µm. (44) Basic micro-sized tools for this method are dicing blades and abrasive pencils (Figure 9) (44) (45).

Dicing blades that have a thickness of 10 µm–1 mm, can be used for precision cut-off grinding. The blades comprise abrasive grains and a sintered or electroplated metal bond. Dicing blades are used for grooving, cutting and dicing different materials. (46)

Abrasive pencil grinding tools are used to create microstructures. Diameters as far as 5 µm can be manufactured. (47) Pencil grinding tools are often used to generate complex three-dimensional micro-sized structures and common applications are form-grinding and jig-grinding (45).

The most frequently used abrasives for micro-grinding are diamond and cubic boron nitride (CBN). CBN has superior thermo-chemical stability compared to diamond. A special type of CBN, ultrafine-crystalline CBN (CBN-U) has even higher wear resistance than ordinary CBN and the grinding ratio is eight times higher. When grinding ferrous components and other materials that react with diamond, CBN is the best abrasive type. (45) It has also been showed that hardened steels can be machined in the micro-scale with CBN-tools (48).

In micro-grinding, due to the small depths of cuts and small grain contact lengths, heat flow into the workpiece and grinding forces are lower compared to conventional grinding. It means, that usage of grinding fluids is not as important as with conventional grinding. (45)

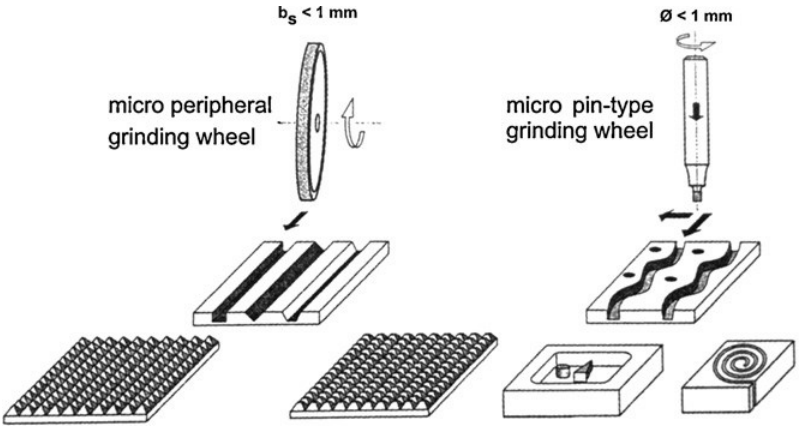

Figure 9. Dicing blade on the left and abrasive pencil on the right. (45)

5.1.7 Mechanical turning

Turning is in many respects the most straight-forward method of metal cutting, which generates cylindrical forms with a single point tool. In most cases, the workpiece is rotating while a stationary cutting tool is fed to remove material. (49)

Turning process is usually carried out with a lathe and can be of four different types such as straight turning, taper turning, profiling or grooving.

These types of turning processes can produce straight, conical, curved or grooved workpieces. Turning means basically generation of external surfaces, whereas the same cutting action when applied to internal surfaces is called boring. Surfaces perpendicular to the rotating axis of the workpiece can also be cut. This operation mode is called either facing or face grooving. (50) Figure 10 illustrates the different types of turning processes.

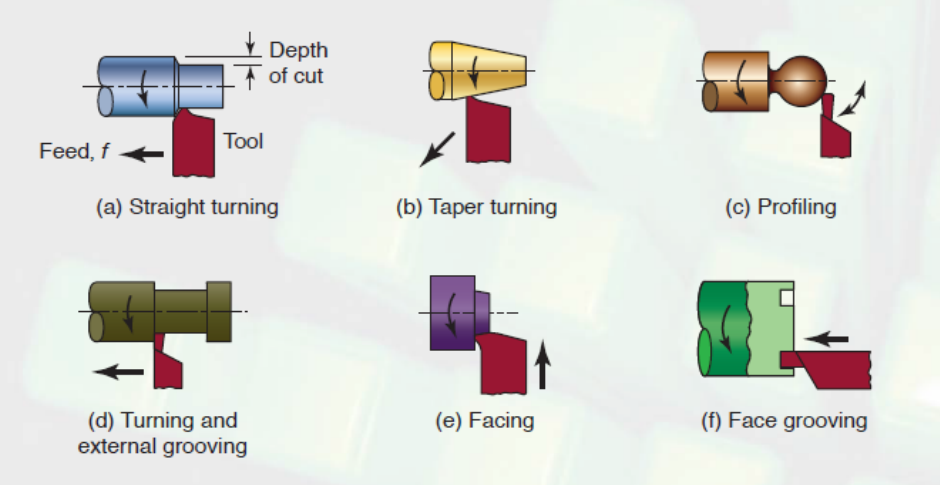

Figure 10. The different turning process types (51)

Micro-turning is an effective way to produce micro-components with cylindrical or rotational symmetry. Micro-parts with high aspect ratio can be achieved by using micro-turning. (52) The process is suitable for producing shafts with diameter of 20–200 µm and small slots by using tailor-made cutters. Micro-turning has wide application fields in industries like automotive, aerospace, electronics and information technology. (53) The biggest drawback in this method is the cutting force which tends to bend the workpiece and therefore it can affect the machining accuracy and limit the machinable size. Micro-turning can be performed on either a conventional precision machine or a micro-turning machine. (52) The process is usually performed with a diamond tool, due to its high hardness, stiffness, thermal conductivity, low friction in air and relative inertness (10).

5.2 Destructive methods

Cross-sections can also be created by causing a controlled fracture to the material. In order to do this, it is important to understand the different fracture types and different factors that affect the fracture of materials. These so called destructive methods can be used to reduce the fracture toughness of a material and to create a fracture to a wanted location.

5.2.1 Fracture types

Fracture is a type of material failure, which is defined as the separation or fragmentation of a solid body into two or more parts under a certain stress. A fracture can be described in different ways depending on the material behaviour and its appearance. Fractures can be classified as ductile or brittle, depending on the ability of a material to undergo plastic deformation during the fracture. Ductile fractures are characterized by considerable amount of plastic deformation before and during the crack propagation.

Ductile metals experience plastic deformation prior to fracture. A brittle fracture instead, is characterized by rapid crack propagation without significant plastic deformation. (54)

5.2.2 Factors affecting the fracture

The main factors that affect the fracture of materials are stress concentrations, speed of loading, temperature and thermal shocks (55).

Stress concentrations

Stress concentrations change the normal stress distribution in materials (Figure 11) (55). Local stress amplification is generally caused by a discontinuity or a notch (56). Therefore, in order to break material, one way is to make a notch in the surface and then apply a force. The amount of the raised stress concentration depends on the depth of the notch and the radius of the notch tip. The deeper the notch and the smaller the tip radius, the greater is the amount by which the stress is increased. A fracture in a ductile material will less likely lead to a failure than in a brittle material. High stress concentration at the end of a notch in ductile materials leads to plastic flow and increase in the radius of the notch tip. This results in decreased stress concentration. (55) (57)

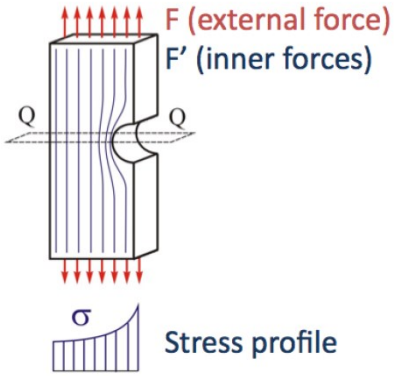

Figure 11. Change in stress distribution caused by a discontinuity. (57)

Speed of loading

Speed of loading can affect the fracture of a material. A sudden impact to the material can lead to a fracture, but if the same stress is applied more slowly a fracture may not occur. With a very high application of stress, there might not be enough time for plastic deformations in a material to occur under normal conditions. In this case, a ductile material will behave like a brittle one. (55)

Temperature

Many metals that are ductile at high temperatures, are behaving like brittle ones at low temperatures. For example, a material may behave as a ductile one above 0 °C, but below that temperature it becomes brittle. This specific temperature is called the ductile-brittle transition temperature. (54) (55) Transition temperature of steels is affected by the alloying elements in it.

Elements like manganese and nickel reduce the transition temperature, while carbon, nitrogen and phosphorus increase it. (55) Figure 12 shows two typical transition-temperature curves for steels.

Ductile-to-brittle transition of metals can be studied by impact testing, where a notched sample is cracked and the absorbed energy during the cracking is measured. The more energy is absorbed by the sample, the more it resists the cracking. The Figure 12 shows that reliance on impact energy at only one point can be misleading. At room temperature, steel A shows higher notch toughness, but its transition temperature is higher than that of steel B. For example at temperature of –20° C the situation is completely opposite. (58)

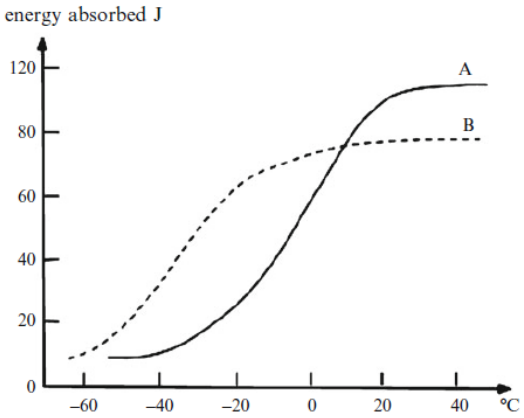

Figure 12. Typical transition-temperature curves for steels. (58)

Thermal shocks

Thermal shocks can induce fracture of materials. For example, when hot water is poured into a cold glass, it can cause the glass to crack. This happens because the surface which is in contact with the hot water expands but is restrained by the colder outer surface of the glass, which is not heating up quickly enough because of the bad thermal conductivity of glass. As a result, the stresses that are built up can be sufficient enough to lead to a fracture. (55)

5.2.3 Impact testing methods

Impact tests are applied to determine the fracture toughness of materials. Testing can be carried out at low temperatures, which means it can also be used to find the ductile-to-brittle transition temperature of materials. (59) An impact test measures how much energy is absorbed by the specimen when it fractures or breaks under a high-speed collision (60). Most common impact tests are done with a pendulum. Most used pendulum tests are Izod-test and Charpy-test. In these methods a notch is often made to the specimen to serve as a stress concentrator. (61)

Izod- and Charpy-test

In an Izod-test, the test specimen is held vertically and the impact usually contacts the the specimen on the notched side.

The orientation of the specimen in a Charpy-test instead, is horizontal and the impact contacts the specimen opposite to the notch side. Figure 13 illustrates the principles of these two tests.

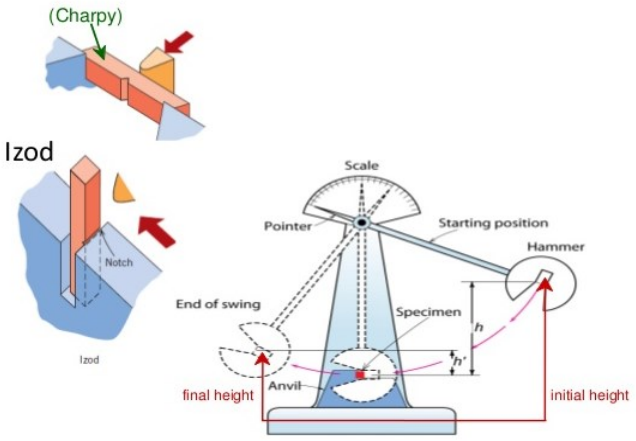

Figure 13. Principles of Izod-test and Charpy-test. (62)

Drop-weight test

Another type of impact testing is a drop-weight test, in which a mass is dropped vertically on to the test specimen. Tubes or rails are used to guide the mass while falling. The dropped mass either stops dead on the specimen or breaks it. The mass and the drop height can be varied either manually or with computer control, depending on the machine. Principle of this testing method can be seen in Figure 14. (60)

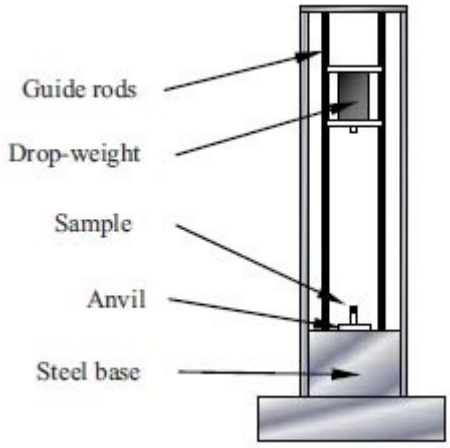

Figure 14. Principle of drop-weight test (63)

5.2.4 Tensile and compression testing methods

Tensile and compression tests are used for predicting the behavior of materials under tensile and compressive loads. (64)

Tensile tests

Tensile tests are used for defining the tensile properties of materials and for predicting the behavior of materials under tensile stresses. A tensile test involves mounting the specimen in a machine and subjecting it to tension. (65) The crosshead speed can be varied to control the strain rate in the specimen. Data from the test are used to define tensile strength, yield strength and modulus of elasticity. (64) The most common testing machines are universal testers, which test different materials in tension, compression or bending. Primary function of the machines is to create a stress-strain curve for the material. Testing machines can be either electromechanical or hydraulic. (65)

Compression tests

Compression test can be used to determine the behavior of materials under a compressive load. Usually compression tests are carried out by placing the test specimen between two plates and applying a force to the specimen by moving the crossheads together. During the test, deformation versus the applied load is recorded. The results are used to determine elastic limit, proportional limit, yield point, yield strength and compressive strength. (64)

In a diametral compression test method, a cylindrical test specimen is compressed between two plates diametrically. As a result of developed tensile stresses, a fracture occurs along the loaded diameter (Figure 15). This method is used to determine tensile strength although it does not develop a uniform un-axial state of tensile stress. Because of its relative simplicity, the test is considerably popular. The specimen aligns itself between the two compressive plates, which means the test can be easily done without additional fixtures. The method is suitable for elevated temperature testing and very small specimens can be used. Compared to other test methods, this test is less affected by surface conditions of the specimen. (66)

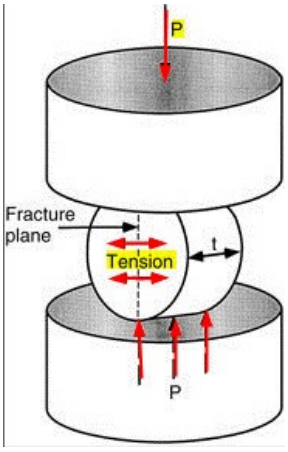

Figure 15. The diametral compression test. (67)

A variation of the diametral compression test is the brittle ring test, which contains a hollow, thick walled specimen instead of a solid cylinder. Loading of the specimen is carried out like in the diametral test method. A steep stress gradient is produced and the maximum tensile stress occurs on the inner surface of the hollow cylinder, at the loaded diameter in the tangential direction (Figure 16). Fracture initiates always in this position and because of the steep stress gradient only a small volume of the specimen is exposed to the maximum tensile stress. (66)

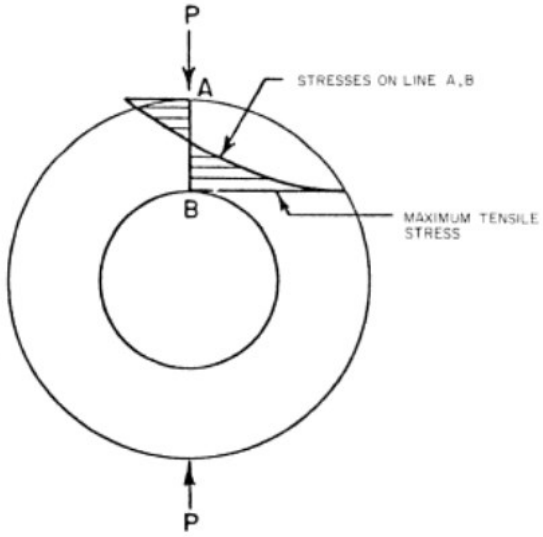

Figure 16. The brittle ring test. (66)

5.3 Non-destructive method

A non-destructive technique for determination of internal geometries in a diesel injector nozzle has been reported. The principle of this technique is to manufacture internal molds from the nozzles by the usage of silicone. The silicone used in the study was vinyl-polysiloxane with a hardness value of 8. This silicone type was giving the best results due to its stretching capabilities and minimum adherence to the nozzle walls. The mold is made by inserting a plastic tube into the nozzle. Introduction of the silicone happens through this tube. Once the silicone is solidified, the mold is pulled very carefully out of the nozzle. (68) Figure 17 illustrates the molding process.

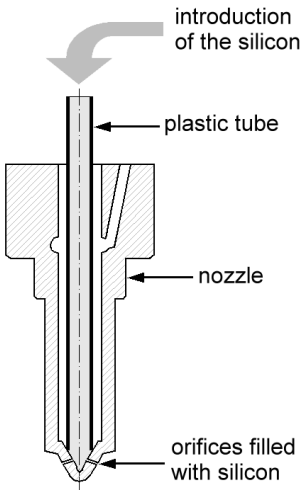

Figure 17. The silicone molding process. (68)

Since this method is non-destructive, the nozzles could be used in an engine afterwards. In the study, the internal geometries of a nozzle are characterized by using an electron microscope (Figure 18). The method has been reported as repeatable. (68)

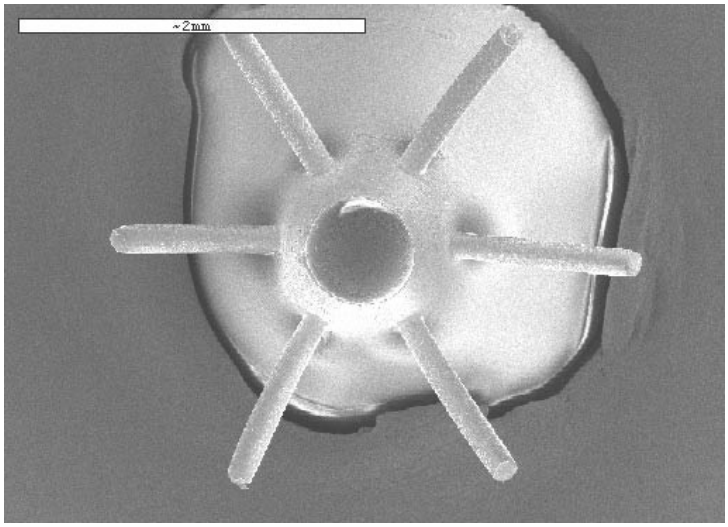

Figure 18. Microscopic picture of the mold. (68)

It was not reported how precisely the silicone material copies the topography of the inner walls. In theory, it would be possible to define the locations of the diesel fuel deposits, if a mold was manufactured before and after the formation of the deposits. By analyzing the topographies of the two molds with an electron microscope, it could be possible to find variations that refer to deposit positions.

6 Selection of methods

For the selection of the methods to be tested, the following factors were evaluated:

- capability of producing the desired conical cross-section
- thermal effects
- speed of the process
- ease of use
- precision
- repeatability
- simplicity
- availability.

Methods that were selected for further testing are listed below:

- laser
- drop-weight testing
- diametral compression testing
- non-destructive silicone molding.

A laser machine capable of micro-cutting was available at KTH. Since laser provides better quality, better precision of cuts and less thermal effects than plasma, the plasma cutting method was left out.

From the impact testing methods, the drop-weight variant was found to be the most suitable and simplest one since the nozzle could be placed in a standing position. A drop-weight testing machine was available at Scania technical center.

Tensile and compression testing machines were also available at Scania technical center. From these methods, the diametral compression testing method seemed to be the most potential one. This method had already been used manually in the current method after the usage of liquid nitrogen. Problem with the tensile testing method was the gripping of the nozzle tip. To make it possible, an additional part for gripping was needed to be attached to the tip, for example by welding, which isn't desirable. Axial compression testing isn't either the best option, because the nozzle tip would probably be totally crushed under the compression.

The silicone molding method was chosen because of its simplicity and availability. The needed silicone material was available at Scania technical center, and the molding process seemed to be fast and easy to perform.

The problem with Ion beam methods was the required processing time and the complexity of the sample preparation. The sample geometry was very limited from the size and thickness. The depth of the cut was so limited, that these methods can be considered more as polishing methods. In addition, the availability of these machines was limited.

EBM and the mechanical machining methods (milling, grinding, turning) would have been potential, but the unavailability of the needed machines and micro-sized tools resulted in leaving these methods out from the testing phase.

7 Tests

The objective of the tests was to find out if the selected methods can be used for injector nozzle sectioning. The tests were carried out for type A and type B nozzles.

7.1 Laser cutting method

The laser cutting method was tested to study its suitability for injector nozzle sectioning. Testing was carried out at KTH by using a Talisker 1000 355-10 picosecond industrial laser machine manufactured by Coherent Inc. Testing equipment consists of a stationary laser gun, a rotating shaft which is inserted inside the nozzle and a controlling software. The vertical and horizontal position, rotating speed and the angle of the shaft can be varied during the cutting process. If needed, the laser can be turned off at wanted positions in the cutting path.

7.1.1 Test preparations

The test preparations consisted of designing a holder for the nozzle and programming a cutting process which would work in a desired way.

Design of nozzle holder

To be able to achieve high precision laser cutting, a holder had to be designed. The holder had to be designed to fit tight inside the nozzle and restrict all the possible nozzle movement to minimum during the process.

The design of the holder and the assembly consisting of the nozzle, holder and rotating tube inside which the holder is inserted, is displayed in Figure 19. The technical drawing of the holder can be seen in Appendix 1. The holder was designed to be a very tight fit, but still some extra friction was needed to keep the nozzle as steady as possible. To create enough friction force between the holder and the nozzle, an o-ring was decided to be used. When the holder is inserted into the nozzle, the o-ring compresses and creates the needed friction force between these surfaces. To make sure the holder is axially in the middle of the nozzle, a conical shape was designed. This shape acts as a wedge, which centralizes the holder when it is pushed as deep as possible inside the nozzle. Because of the friction force produced by the o-ring and the centralizing effect of the wedge, the nozzle should stay still while this assembly is rotated in nearly horizontal position.

The part of the holder placed inside the rotating tube was also designed to be a very tight fit. A conical shape that acts as a wedge was designed for the centralizing purpose. The final tightening could be done with a screw, which goes through the wall of the rotating tube. Due to a misunderstanding in the machining workshop, instead of the wanted conical shape in this part of the holder, a straight surface was machined. The holder was manufactured from steel.

The inner diameter of the used o-ring was 4.5 mm and the outer 8.5 mm. The used material was nitril rubber.

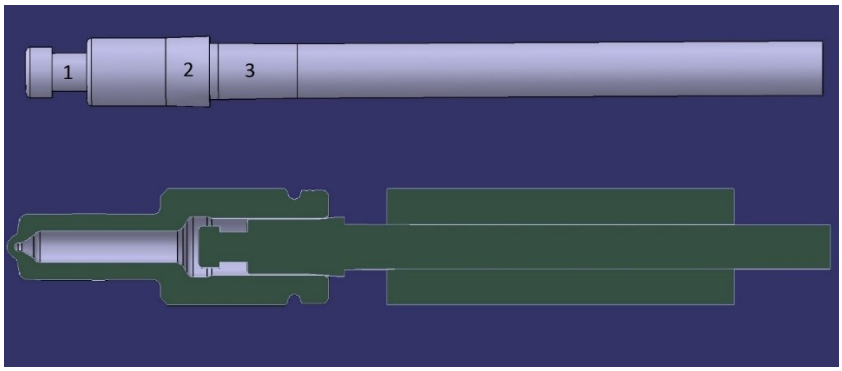

Figure 19. The design of the holder and a cross-section from the test assembly. In the holder design, the groove for the o-ring (1), the wedge going inside the nozzle (2) and the wedge going inside the rotating tube (3) are presented.

Program for the cutting process

The cutting process was programmed by using Spyder, which is a Python development environment. The program was made to work in a way that the laser beam was turned off every time it crosses a hole, because a contact between the laser beam and the deposits had to be avoided. Before cutting, the used laser parameters, the amount of rounds, the rotating speed, the cutting angle and the desired groove width were fed to the program.

Since the distance between two holes has a certain tolerance, the positions of the holes had to be defined manually and fed to the program prior to cutting. The safety gap between a hole and the cutting groove could also be defined to avoid any thermal effects to the walls of the spray-holes and to the deposits.

The groove width function is illustrated in Figure 20. If set to 1, the laser beam follows the same path round after round. If instead, a value of 3 is used, the beam moves one step along the x-axis after every round, which means that the beam would have returned to original x-position after six rounds. In theory, the width of the final groove would be close to 3 times the width of the laser beam. The idea behind the groove width function was to try if there were significant differences in the groove quality and groove shape between different used groove width values.

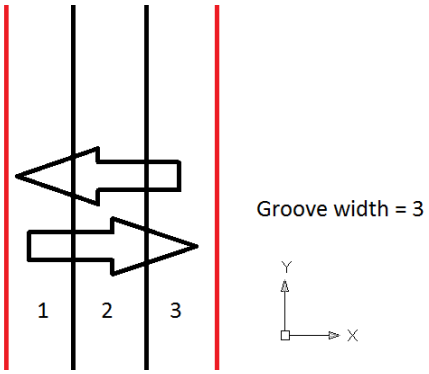

Figure 20. Principle of the groove width function.

7.1.2 Testing

To get a better understanding about the right range of parameters, multiple test grooves were made to several nozzles (Figure 21). Different laser intensities and different groove widths were used in order to find the optimal combination between groove quality, thermal effects and processing time. During the tests, thermal behaviour of the nozzle tip was monitored with an infrared camera. After testing, cross-sections were made across the grooves to study and measure the results with Scanning Electron Microscope (SEM).

The main parameters that were tested with different values and combinations are listed below:

- frequency (tells how often a certain chain of bursts should be shot)
- burst length (the number of bursts the laser will shoot when it is triggered)
- groove width

The parameters that were kept constant are listed below:

- AmpRep Rate = 500 kHz (maximum repetition rate for the laser)
- Attenuation = 0 (laser pulse has the highest possible energy)
- AOM = 1 (every pulse is picked. If value is 2, every second pulse is picked etc.).

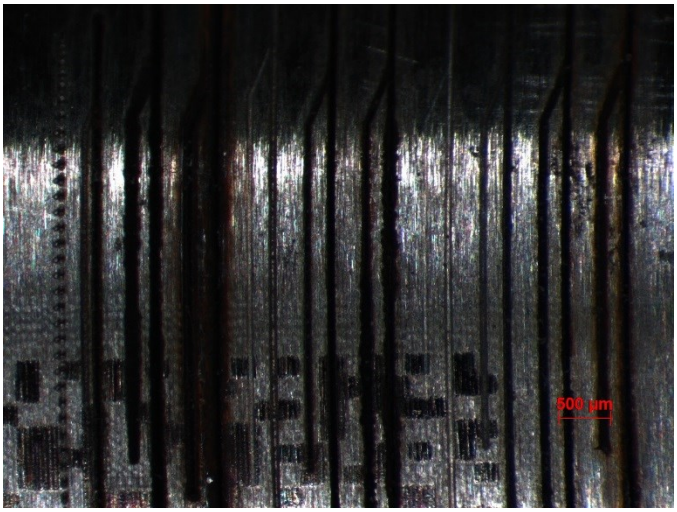

Figure 21. Test grooves made to a nozzle with different parameters (LOM).

Tips of three type A nozzles and one type B nozzle were also cut to examine the precision of the process and the designed holder. The other purpose of these cuts was to create a notch to these nozzle tips, and test if the notch provided any benefit in the destructive methods.

7.2 Drop-weight method

The objective of this test was to examine if a drop-weight testing machine could be used for injector nozzle sectioning. The idea was to use the needle, which is operating inside the nozzle and is manufactured to be a perfect match for the inner nozzle geometries, as a connecting part between the nozzle tip and the dropped weight. The weight was to be dropped on the needle, resting inside a standing nozzle. The dropping weight creates an impact force, which travels to the nozzle tip through the needle, creating a sudden tensile force.

7.2.1 Test preparations

The made test preparations consisted of estimations of the needed and available impact force and estimation of the needed dropping height. In addition, a special platform for the nozzle and three different needle modifications were designed.

Needed and available impact force

Before testing it was necessary to estimate the magnitude of the needed force to break the material.

In mechanical designing processes it is important to ensure, that the strength of the mechanical element will always exceed the stress which is exerted on it due to any kind of load. In designing processes, an assumption of uniform distribution of stresses is frequently considered. (69) The needle will create an axial load F to the nozzle tip, which has a cross-sectional area A. And if σ is considered as the tensile stress acting on the cross-sectional area, the magnitude of the uniformly distributed force can be calculated as follows:

$$F = \sigma A. \tag{1}$$

In order to estimate the needed force, the tensile stress and the cross-sectional area had to be defined for this particular case. Since the material has to break entirely, the needed value for σ is the ultimate tensile strength of the nozzle material. The cross-sectional area of the nozzle tip can be easily defined by using Catia V5 modeling program. For this purpose, a CAD-file of a nozzle without spray-holes, that was available for this project, was used. The cross-sectional area of the tip is clearly the smallest in the whole injector nozzle, which makes it the weakest spot even without the spray-holes. The spray-holes are considered as discontinuities that create local stress concentrations, so it was concluded that the actual needed force could be even smaller than the one defined in this estimation. Estimation of the needed force was calculated for two different scenarios. Calculations were made for a "simplified nozzle" and a more exact nozzle in order to have an understanding of the range for the needed force.

In the simplified nozzle scenario it was assumed that the nozzle tip would have the same cross-sectional area as the shaft before it (Figure 22).

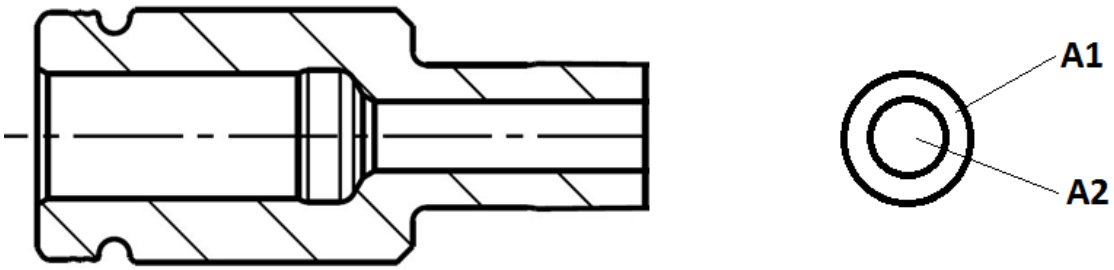

Figure 22. The cross-section of the simplified nozzle.

By using the dimensions from the technical drawing of the nozzle, the cross-sectional area was calculated as follows:

$$A_{\text{circle}} = \pi r^2 \tag{2}$$

$$A_{cross-section} = A_1 - A_2$$

By using the ultimate tensile strength and the cross-sectional area, the needed force was calculated using equation 1 as follows:

$$F_{simplified} = 117\ kN$$

The cross-sectional area of the nozzle tip cannot be calculated easily with the help of the technical drawing. Therefore, the 3D-model was used. The 3D-model of the nozzle was cross-sectioned from the tip, and the surface area of the cross-section was calculated by using the "Measure Inertia"-tool of Catia V5. Using these values, the needed force was calculated using equation 1 as follows:

$$F_{more\ exact} = 20925\ N$$

The next problem was to estimate the maximum impact force that the available drop-weight machine could provide. When an object is dropped from rest, its gravitational potential energy (PE) is converted to kinetic energy (KE). Gravitational potential energy of a mass is calculated as follows:

$$PE = mgh, \tag{3}$$

where m is mass, g is gravitational acceleration and h is height.

Kinetic energy of the mass is calculated as follows:

$$KE = \frac{1}{2}mv^2, \tag{4}$$

where *m* is mass and *v* is velocity. Since the principle of work and energy is formulated as follows:

$$\frac{1}{2}mv_1^2 + mgh_1 = \frac{1}{2}mv_2^2 + mgh_2, \tag{5}$$

and the velocity v_1 and the height h_2 are equal to zero in this application, it can be stated, that for a simple drop-weight application:

$$mgh_1 = \frac{1}{2}mv_2^2, \tag{6}$$

where h_1 is the drop height and v_2 is the velocity at impact. During the impact, the work done (W) is equal to the average force of impact ($F_{average}$) multiplied by the distance traveled after the impact (d):

$$W = F_{average}d. \tag{7}$$

Since the work done on a particle as it moves between two positions equals the change in its kinetic energy, the work done in a drop-weight application can be expressed as follows:

$$W = \frac{1}{2}mv_2^2 - \frac{1}{2}mv_1^2. \tag{8}$$

Because the initial velocity v_1 is equal to zero,

$$W = \frac{1}{2}mv_2^2. \tag{9}$$

When equations 6, 7 and 9 are combined, the average impact force can be calculated as follows:

$$F_{average} = \frac{mgh_1}{d}. \tag{10}$$

The distance traveled at the impact (d) has to be estimated. The distance estimation is depending on whether a perfectly elastic collision occurs or not. Perfectly elastic collision in drop-weight testing means that there is a perfect rebound after the impact.

This can be explained in a way that first a steel ball is dropped from a certain height onto a foam pad. Since the ball penetrates the material, energy is absorbed and the impact force is minimized. In this case, the value d is relatively large. On the other hand, if the steel ball is dropped on to a steel plate, it may even rebound back to the same height and a very little amount of energy is absorbed. In this case, the impact force is very high, value d close to zero and a collision which is near to a perfect elastic collision has happened. (70)

The planned drop-weight application includes a steel-to-steel collision, leading to a large impact force. An estimation of 0.0001 m traveling distance has been previously proposed in a steel-to-steel collision during drop-weight testing (70).

The upper limit for dropped mass is 2 kg and the drop-height 1 m in the available machine. Using these values, the maximum average impact force that can be provided is calculated by using the equation 10:

$$F_{average} = \frac{2kg * 9.81\ \frac{m}{s^2} * 1\ m}{0.0001\ m} = 196\ 200\ N$$

This means that the estimated maximum impact force that can be applied to the needle is approximately 196 kN.

Equation 10 shows that the value of the average impact force is highly dependent on the value d. For example if d is changed to 0.0005 m, the average impact force would reduce to approximately 39 kN.

Needed dropping height

When the needed forces $F_{simplified}$ and $F_{more\ exact}$ are known, the dropping height can be calculated by using the equation 10. The estimated height was calculated for the simplified and the more exact tip scenario as follows:

$$h_{simplified} = \frac{117000\ N * 0.0001\ m}{2\ kg * 9.81\ \frac{m}{s^2}} = 0.596\ m$$

$$h_{more\ exact} = \frac{21000\ N * 0.0001\ m}{2\ kg * 9.81\ \frac{m}{s^2}} = 0.107\ m.$$

Design of nozzle platform

In order to keep the nozzle in a vertical position, a special platform had to be designed. It was vital that the central axis of the nozzle and the needle would be coaxial with the central axis of the dropped weight, which is a shaft in this particular machine. The original setup of the drop-weight machine can be seen in Figure 23.

The drop-weight is released from a certain height and guided to the center of the hole which is in the original platform. As can be seen, the hole and the drop-weight are coaxial. This could be exploited in the design of the platform.

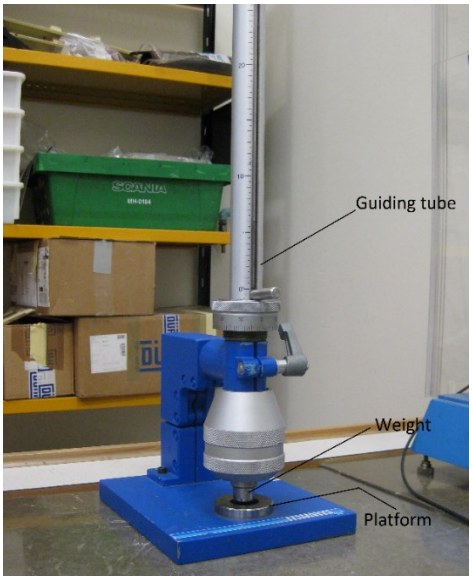

Figure 23. The original test setup.

A platform as shown in Figure 24 was modeled with Catia V5 modeling program and the compatibility of the involved parts was tested in assembly design. For this purpose, the original platform of the drop-weight machine was measured and then modeled. With cross-sectioning and clash detection tools it was assured that the assembly didn't have any overlapping surfaces.

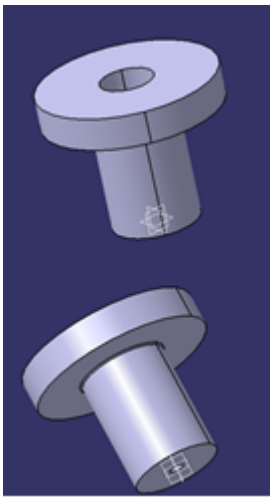

Figure 24. Designed platform for the drop-weight test.

To ensure that the platform was strong enough for the application, a basic stress-analysis was made by using Generative Structural Analysis –tool in Catia V5. The platform was restrained in the same way it would be in test conditions and a rigid virtual part was created inside to simulate the presence of the nozzle. A distributed force of 21 kN, which was previously calculated to be the estimated maximum load for the nozzle tip fracture, was created to act downwards through the rigid virtual part to simulate the impact force created by the drop-weight. Figure 25 illustrates the setup of the analysis.

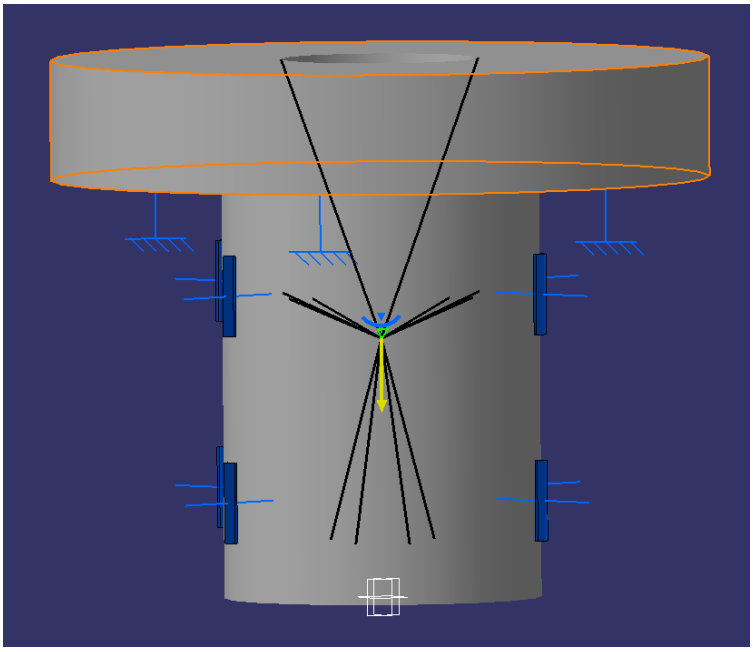

Figure 25. Setup for the stress analysis. Black lines represent the rigid virtual part and yellow arrow represents the impact force acting through it. Blue marks on the lower surface of the flange tell that the part is clamped from that surface, and the other blue marks on the lower shaft simulate that there is a sliding surface against that shaft surface.

Average properties of steel (71) were used to determine the material in order to achieve a general understanding how the designed platform would behave under the force. The used values can be seen from Figure 26.

Material	Steel
Young's modulus	2.1e+011N_m2
Poisson's ratio	0.3
Density	7830kg_m3
Yield strength	0N_m2
Coefficient of thermal expansion	1.2e-005_Kdeg

Figure 26. Material properties fed to the analysis. Yield strength can be defined for means of comparison, but is not mandatory since it doesn't affect the result of the analysis.

Results of the analysis showed the magnitude and locations of the developed von Mises stresses (Figure 27). The maximum value of stress was ~150 N/mm², which means that the yield strength of the chosen material had to be larger than that. To ensure the material wouldn't fail, a factor of safety was decided to be at least 2. This means that the chosen material had to have a yield strength of 300 N/mm² or more.

Based on the availability in the machining workshop at Scania with sufficient mechanical properties, Steel type SS2541, equivalent to 34CrNiMo6 (standard SS EN10083-3/EN10277-5) was chosen.

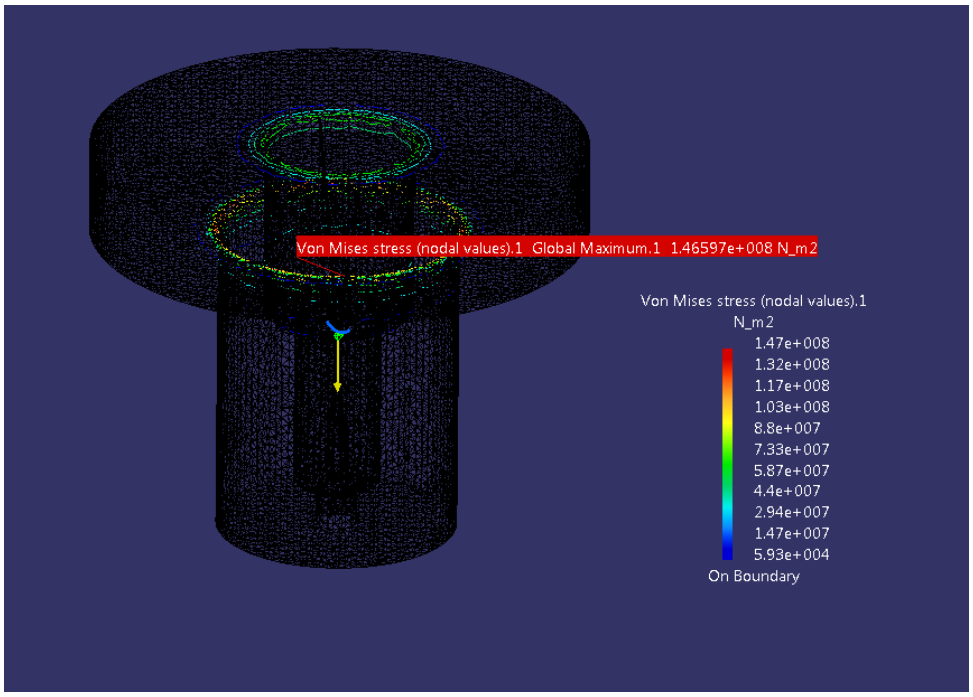

Figure 27. Result of the stress analysis.

Design of modified needle

Prior to testing it was concluded that the usage of original needles might create undesired results. The possible problem was the fact that the needle is not in contact with the nozzle tip. The contact between the needle and the nozzle is at a higher level than where the force is wanted, which might cause the fracture to happen elsewhere.

In order to create a contact between the needle and the nozzle only at the tip, a different needle had to be designed. The geometry of the needle tip was re-designed and the compatibility with the nozzle was tested in Catia V5 assembly environment. There was no need to design the whole needle again, so the original ones were modified only from the tip by grinding. After grinding, the needles were shortened from the other end.

Three needle tip types with different dimensions were designed for testing. The technical drawings can be seen in Appendix 2.

7.2.2 Testing

In order to make the test machine stable, it was clamped to the table. The metallic collar around the weight shaft was screwed down and tightened against the designed nozzle platform. A plastic transparent cup was taped under the platform to collect all the pieces that could possibly drop out through the bottom hole of the platform. The weight was lifted manually to certain height and then released. After every impact, conditions of the needle, nozzle and the platform were checked. Prior to testing, the needles were cut shorter. The test setup is presented in Figure 28.

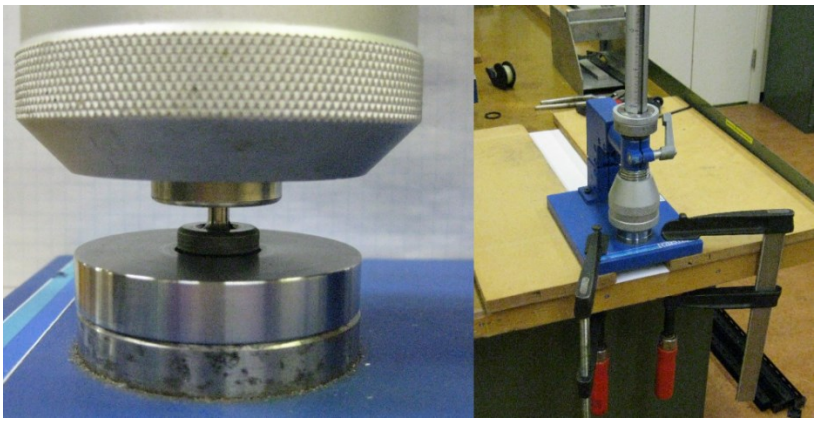

Figure 28. Test setup for drop-weight method.

Several un-used and used type A nozzles were tested. One of the used type A nozzles was notched with laser. In addition, two un-used and un-notched type B nozzles were tested. Testing was done with all the different needle types, including the original and the different modified needles. Table 1 shows all the different combinations used in the tests.

Table 1. Different combinations used in the tests.

Nozzle type	Notched/Un-notched	Used/Un-used	Needle type	Tested amount
Type A	Un-notched	Un-used	Original	2
Type A	Un-notched	Un-used	Modified type 1	3
Type A	Un-notched	Used	Modified type 1	5
Type A	Notched	Used	Modified type 1	1
Type B	Un-notched	Un-used	Modified type 1	2
Type A	Un-notched	Un-used	Modified type 2	2
Type A	Un-notched	Un-used	Modified type 3	2

7.3 Diametral compression method

The aim of the diametral compression tests was to study if the current method developed by Scania could be done without the usage of liquid nitrogen and a manual press. The usage of liquid nitrogen increases the risk of deposit contamination and removal, while the usage of manual press makes the process unstable.

7.3.1 Test preparations

Test preparations included an estimation of the needed force and finding a suitable machine based on the estimation. In addition, one used and laser-notched type A nozzle was tested with the current sectioning method. The nozzle was frozen with liquid nitrogen and then compressed diametrically in a manual press. The purpose of this test was to create a reference result, which could be compared to the results achieved with the diametral compression method.

Estimation of the needed force

In order to find a suitable compression test machine, an estimation of the needed compression force was needed. The maximum tensile stresses acting uniformly across the loaded diameter are given by:

$$\sigma_t = \frac{2P}{Dt\pi}, \tag{11}$$

where P is the applied load, D is the cylinder diameter and t is the cylinder length.

This analysis is valid for solid cylinders, which means it cannot be used directly for an application of diametral compression of an injector nozzle. The nozzle is a hollow cylinder which has basically a cross-section of a ring disc. Considering a ring disc subjected to diametrical loading, the object consists of two surfaces with external (T_1) and internal (T_2) boundaries (Figure 29) (72).

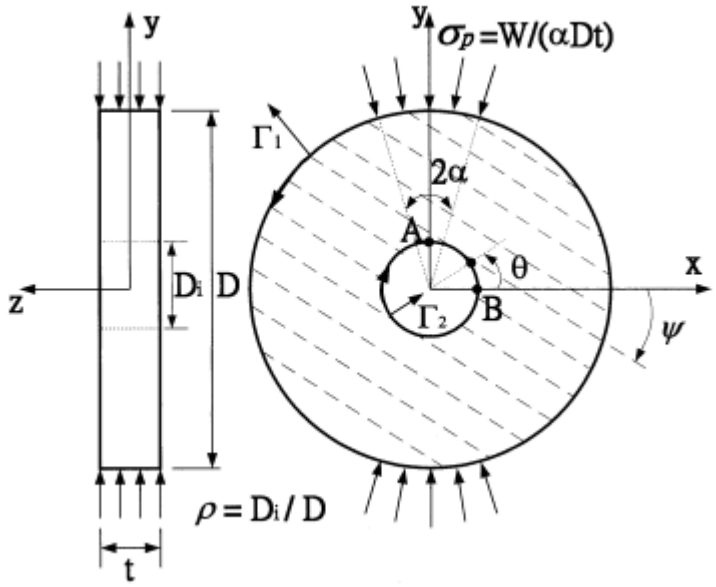

Figure 29. A ring disc subjected to diametrical loading. **(72)**

In a ring disc application, the loading angle 2α is assumed to be small so that the applied diametrical traction is given by:

$$\sigma_p = \frac{W_y}{\alpha D t}, \tag{12}$$

where W_y is the force applied in the y direction, D is the outer diameter of the ring and t is the thickness of the disc. At any point within the disc, the components for of the stress field are given as follows:

$$\sigma_x = K'_{xx}\frac{W}{\pi D t},\ \sigma_y = K'_{yy}\frac{W}{\pi D t},\ \tau_{xy} = K'_{xy}\frac{W}{\pi D t},$$

where $K'_{xx}, K'_{yy}, K'_{xy}$ are stress concentration factors. Based on investigations, the maximum tensile stress acts at point A and the maximum compressive stress at point B (Figure 29 above). The value of tensile stress acting at point A can be expressed as follows:

$$\sigma_x = K_{xx}\frac{W}{\pi D t}, \tag{13}$$

where K_{xx} is the stress concentration factor at point A.

If an assumption is made that the indirect tensile strength (σ_t) is given by the maximum absolute value of the stress σ_x at point A, it can be defined that:

$$\sigma_t = K_{xx} \frac{W_f}{\pi D t}, \tag{14}$$

where W_f is the load when specimen fails. (72) The maximum tensile stress around a hole when an isotropic ring is subjected to concentrated line loading has previously been investigated and an approximate solution has been proposed as follows:

$$\sigma_t = 12 \frac{W_f}{\pi D t}. \tag{15}$$

A more exact solution, which considers the influence of the size of the hole, has also been previously presented as follows:

$$\sigma_t = (12 + 76_{\rho^2}) \frac{W_f}{\pi D t}, \tag{16}$$

where ρ is the ratio between internal and external diameter of the ring. These two equations can be used for determining the tensile strength of isotropic rings under line loading. It has been studied that the approximate values of stress concentration factor K_{xx} given in the equations are in good agreement with practical test results, except for large values of ρ.

The studies showed that the difference between the approximation and the studied result starts to increase when ρ > 0.3. The maximum value of ρ in the study was 0.4 and the studied value for that was 27.06. The approximation formula for K_{xx} instead, gives a value of 24.16, which means the difference between these two values is 2.9. Figure 30 illustrates the recorded results in the study. The lower row represents the studied values while the upper one shows the values calculated with the approximation formula. (72)

$\rho = 0.1$	$\rho = 0.2$	$\rho = 0.3$	$\rho = 0.4$
12.76	15.04	18.84	24.16
12.67	15.07	19.52	27.06

Figure 30. Examined and calculated values for K_{xx} . (72)

Since the available compression test machine consists of two flat plates that are pressed against the cylinder-shaped nozzle, a line contact loading can be assumed (73). The diameter of the nozzle varies along the length, which means the compression plates will be pressed against the section where the diameter is largest (Figure 31).

In order to avoid this, the nozzle can be cut in a way that the section which has the smaller diameter is separated and placed between the compressive plates.

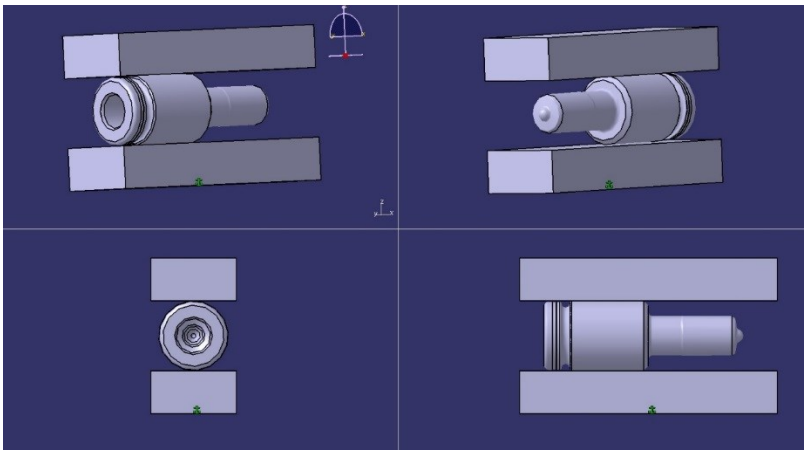

Figure 31. Contact between the nozzle and the compressive plates when the nozzle is not modified.

Equations 15 and 16 were both used to estimate the needed force. The load needed for specimen failure (W_f) can be solved from equations 15 and 16:

$$W_{f\,approximate} = \frac{\sigma_t \pi D t}{12}\,, \tag{17}$$

$$W_{f_{more\ exact}} = \frac{\sigma_t \pi D t}{(12+76_{\rho^2})}\,. \tag{18}$$

The W_f gives values of:

$$W_{f\,approximate} = 120\,519\ \text{N}\,,$$

$$W_{f_{more\ exact}} = 49\,190{,}3\ \text{N}.$$

The results are different, but it can be deduced that the available compression test machine, which has an upper force limit of 600 kN, can be used for the tests. It should be mentioned, that the equations 15 and 16 are usable for diametral loading of hollow cylinders and the nozzle is not completely hollow, since the other end is closed with a dissimilar geometry compared to the open end. Due to this, it can be assumed that the crack will initiate from the open end and progress along the longitudinal axis towards the closed end of the nozzle.

7.3.2 Testing

Before testing, all the nozzles were shortened like shown in Figure 32.

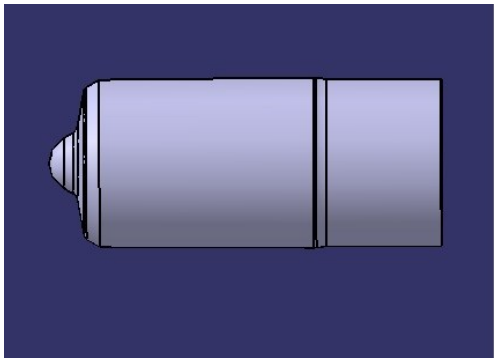

Figure 32. Shape of a shortened nozzle.

The test machine setup is shown in Figure 33. The nozzle was placed between the compressive plates in a way that the tip was visible to the machine operator. To make it easier to collect the fractured pieces, it is recommended to put the nozzles inside a plastic bag.

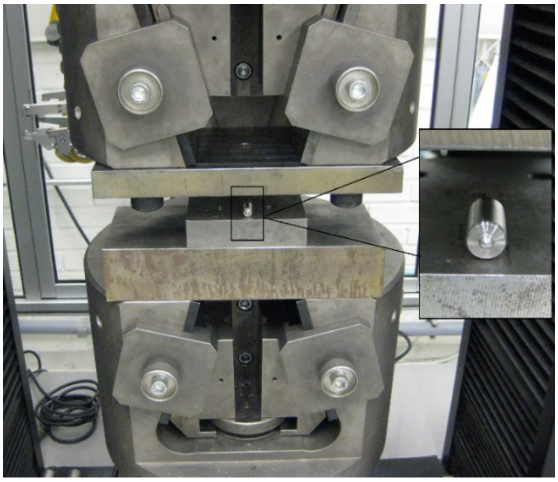

Figure 33. Diametral compression test setup.

Tests were carried out for type A and type B nozzles. Tested type A nozzles included unused and used ones that were either un-notched or notched. The used type B nozzles were un-used and either un-notched or notched. All the notches were made with laser. Different loading speeds were used during the tests to study if it has any influence on the resulted fractures. Table 2 shows different nozzle types that were tested.

Table 2. Tested nozzle types.

Nozzle type	Notched/Un-notched	Used/Un-used	Tested amount
Type A	Un-notched	Used	8
Type A	Un-notched	Un-used	3
Type A	Notched	Un-used	1
Type B	Un-notched	Un-used	1
Type B	Notched	Un-used	1

7.4 Silicone molding method

The aim of this test was to study if the locations of injector nozzle deposits could be defined by using a silicone molding material. A mold, which replicates the topography of the internal surfaces in a nozzle, was made from an un-used type A and used type A nozzle, which had deposits in it according to previously made fuel flow tests.

7.4.1 Mold material

The material used for molding was Stuers RepliSet F1, which is a fast curing two-part silicon rubber used for making flexible high-resolution 3D-replicas. The material can be studied with an optical microscope. It is applied by using a dispensing gun, which is combined with a mixing nozzle.

Replicas made with the RepliSet F1 have a dimensional accuracy for measurement purposes. A replica can be taken of all metallic materials. (74)

7.4.2 Molding process

The nozzle was held manually in a vertical position with nozzle holes facing the ground. The mixing nozzle of the dispensing gun was set inside the injector nozzle in a way that it was as close as possible to the tip. The molding material was injected inside the injector nozzle and when it started flowing out of the nozzle holes, it was pulled out slowly while injecting at the same time. To avoid any air inclusions in the mold, the dispensing gun should be pulled out in a way that it is submerged under the top level of the molding material until the whole injector nozzle is filled.

After the filling, a backing paper was pressed against the top level of unsolidified molding material. The backing paper adheres to the material and enables removing of a solidified mold by pulling it away from the injector nozzle. To make sure that the mold is fully solidified, a curing time of 20 minutes was used. A finished mold can be seen in Figure 34.

Before detaching the mold from the injector nozzle, a tiny scalpel was used to cut away all the excessive material which had flown out from the nozzle holes. If this is not done, the excessive material which is attached to the outer surface of the injector nozzle tip would tear some of the important nozzle holes apart from the mold while the solidified mold is pulled out.

A finished mold was wrapped in the backing paper and put into a plastic bag to prevent dust sticking to the mold surface. The mold cannot be in direct contact with plastic due to possibility of plastic particles sticking to the mold surface.

Figure 34. A finished silicone mold.

8 Test results

8.1 Laser cutting method

8.1.1 Parameters

The cross-section from a nozzle with multiple grooves (chapter 7.1.2) was studied with SEM. In every groove, the laser beam had made 10 passes along the same line. The achieved groove depths and widths are presented in Table 3.

Table 3. Test results with different parameters.

Burst length	Frequency [Hz]	Groove width [µm]	Groove depth [µm]
50	1 000	45,70	252,7
50	10 000	94,02	406,8
10	10 000	74,43	305,6
2	10 000	37,22	212,2
2	100 000	56,15	319,3

The results tell that the depth and the width can be controlled by adjusting the values of burst length and frequency. If the burst length is kept constant, the higher the frequency is, the deeper and wider the groove will be. If the frequency is kept constant, the higher the burst length value is, the deeper and wider the groove will be.

When the different scenarios in the Table 3 are compared, the best parameters in terms of groove width and processing time can be achieved with a burst length value of 2 and frequency value of 100 000 Hz. The SEM-pictures taken from this groove are presented in Figure 35.

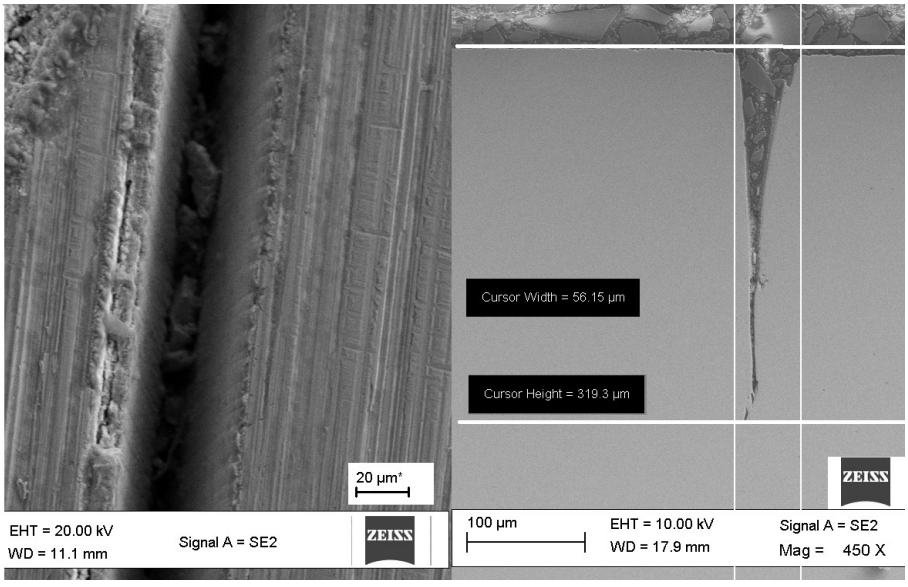

Figure 35. SEM pictures taken from the groove made with burst length of 2 and frequency of 100 000 Hz.

In the second set of tests, different groove widths were used and the cross-sections were studied with Light Optical Microscope (LOM). Differences were seen between different groove widths. The example shown in Figure 36 was cut with a groove width of 6. The bottom width of the groove was clearly closer to the width of the top than in the cuts done with groove width value 1. The trend was similar in the cross-sections that were cut with a groove width value of 3.

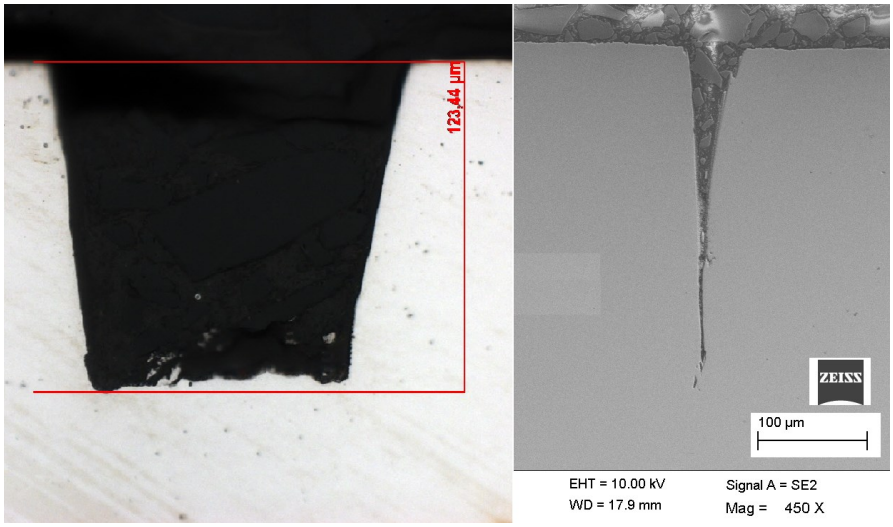

Figure 36. A groove obtained with groove width of 6 on the left (LOM). A groove obtained with groove width of 1 on the right (SEM).

8.1.2 Holder

The cutting process was tested with an existing holder, which showed results that did not provide acceptable outcomes in terms of precision and repeatability. Figure 37 shows that the nozzle has clearly moved during the cutting process, resulting in 2 or 3 separate grooves instead of one uniform groove.

Results with the new holder model, which was designed to meet the needs of stability and precision, were significantly better. The beam seemed to follow the exact same path in every cutting round, giving one uniform groove without any abnormalities. The combination of the o-ring and the wedge gave the stability needed in order to create high-precision laser cuts.

Figure 37. Type A nozzle tip cut by using the old holder model.

8.1.3 Thermal effects

The temperature of the nozzle tip was monitored with infrared camera during the tests. Even with highest laser intensity, there were no signs of global temperature rise in the material outside the cutting groove.

8.2 Drop-weight method

8.2.1 Original needles

Two original needles were tested together with type A nozzles. The needles were capable of breaking the nozzle, but as it is shown in Figure 38, the fracture does not occur in the desired position. Like it was assumed prior to testing, the position of the surface contact between the needle and the nozzle is causing problems. In both tests, when the weight was dropped from a height of 0.45 m, the needle got stuck inside the nozzle. Below this particular height there were no signs of fracture in the components. In the first test, the dropping height was increased step by step to the maximum height provided by the machine, which was 0.92 m. Still there were no signs of fracture in the nozzle tip, which could be seen from the bottom hole of the platform. When the nozzle was withdrawn from the platform it was observed that it had fractured in some point of the test. A second test proved this fracturing height to be 0.6 m.

The position of the fracture was in a place where the cross-sectional area of the nozzle is the same that was used in the simplified nozzle calculations previously. The result showed that the calculated dropping height of 0.596 m was close to reality. The first test confirmed, that the designed platform is capable of receiving the maximum impact force provided by the machine without any damages.

Figure 38. Result when original needles were used.

8.2.2 Modified needles

From the modified needles, type 1 produced the best results. Type 2 and 3 were too fragile at the tip. The tips fractured every time between dropping heights of 0.15–0.2 m, after which the needles could not be used for the application.

Type A nozzles

Figure 39 presents some of the results that were achieved with un-notched type A nozzles by using modified needle type 1. From the eight tests that were made, seven produced the desired conical cross-section. The eight one failed because the used needle had already been used in three previous tests and was too damaged to create any fracture to the nozzle. Therefore, it seems that the same needle can be used only three times.

The resulting conical cross-sections had basically the same shape every time and almost every hole was exposed. In some of the tip cross-sections, one or two holes were not fully visible. The reason might be due to the process variations between the nozzles and the needles.

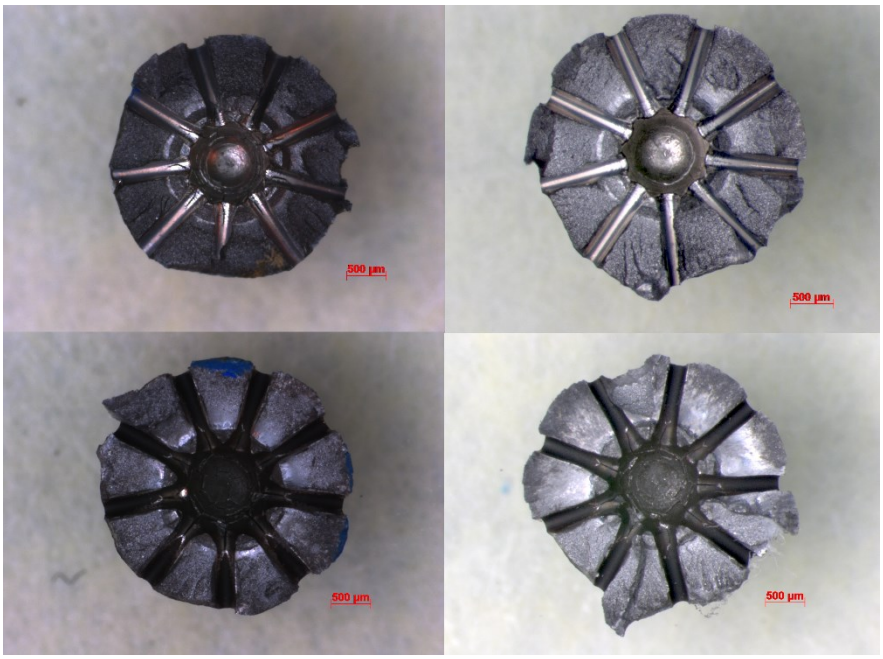

Figure 39 Upper row: un-used nozzles, lower row: used nozzles

Due to the testing machine design, it was not possible to set a lower limit for the weight, where it would stop. This gave the results, that when the nozzle tip cracked and fell off, the weight still forced the needle downwards, until the nozzle platform stopped it. Assumably because of this, the tapered surface of the needle collided with the tapered surface of the nozzle like in the first tests made with original needles. This caused another fracture to the nozzle from the same spot than in the first tests with the original needles.

The separated part, containing the other halves of the holes, fractured differently every time (Figure 40). This can be considered as a drawback, but still most of the holes were visible, and all the parts could be collected from inside of the test platform.

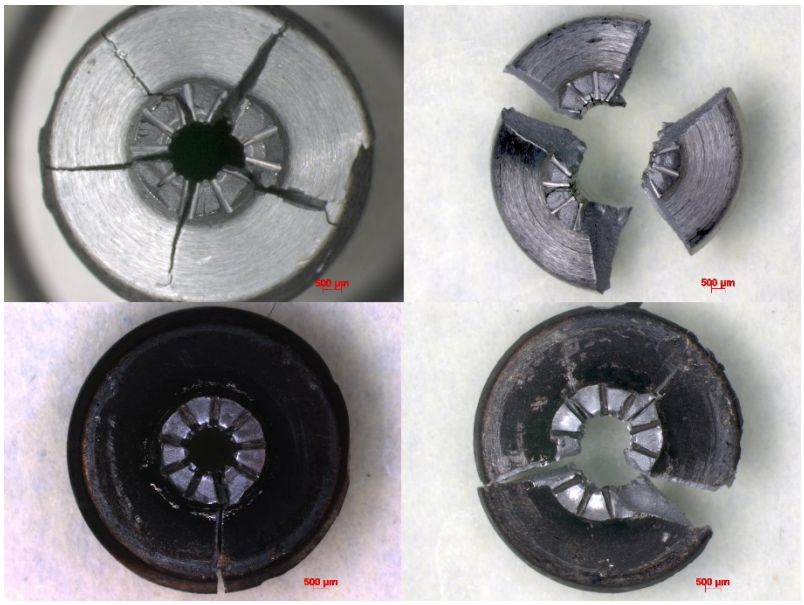

Figure 40. Examples of other halves of the holes. Upper row: un-used nozzles, lower row: used nozzles.

The results were partly unexpected because of this second fracture and the needed dropping height. The calculated estimation suggested that the needed dropping height would be in a region of 0.11 m. When the weight was dropped from 0.15 m, the needle only got stuck inside the nozzle without breaking it. For the three un-used and un-notched type A nozzles that were tested, the needed height turned out to be 0.55 m. In every test, the needle was already stuck inside the nozzle until the fracture happened. For the used and un-notched nozzles, a height of 0.65 m was needed. After the breakage it could be seen that the needle tip was clearly compressed and deformed (Figure 41), which could be one reason for the unexpectedly high dropping height.

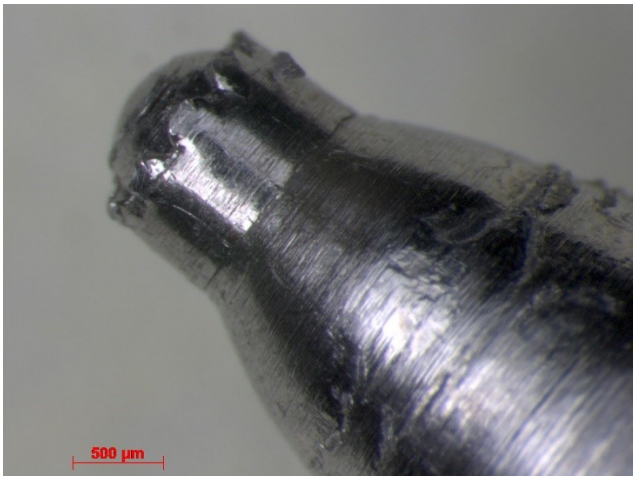

Figure 41. Deformed needle.

Like mentioned previously, one needle was used for four different nozzles. The needle broke the tip in the wished manner three times, until it wasn't able to break a nozzle at all, not even when dropped from the maximum height of 0.92 meters. It was observed that the second and third times, a dropping-height of 0.8 m was required to create a fracture.

The first three times produced similar conical tip cross-section, but like in all the other successful tests, the second fracture that occurred in the higher level, produced dissimilar amount of pieces.

The cross-section achieved with the used and notched type A nozzle was similar to the ones with un-notched nozzles. Only difference was the reduced dropping height of 0.5 m.

Type B nozzles

The two un-used and un-notched type B nozzles offered results that can be seen from Figure 42. The tip cross-sections do not reveal all the holes and the shapes of the cross-sections are slightly different. The cross-sections of the other halves are again fractured to multiple pieces like with the type A nozzles.

In both tests, the needle got stuck inside the nozzle when the weight was dropped from 0.5 m. The needed dropping height for a fracture was 0.7 m in both tests.

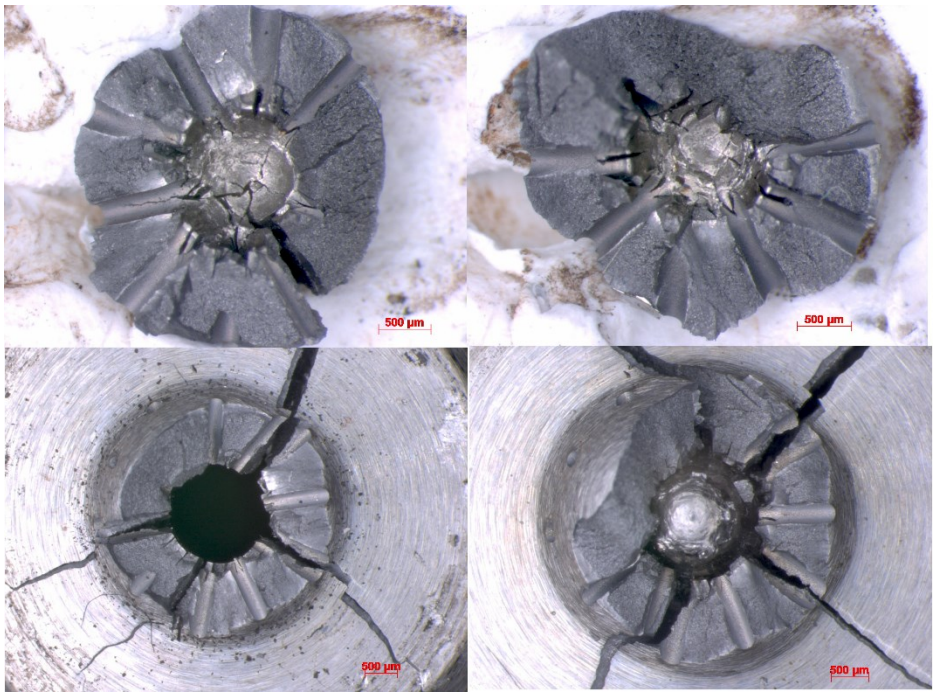

Figure 42. Fractured type B nozzles.

Effect of the original needle design

The drop-weight method was tested 17 times in total, with different needle types. In seven cases, the needle remained stuck inside the nozzle even after the nozzle had fractured from the tip. In rest of the cases, the needle could be withdrawn from the nozzle after the fracture had happened. It was detected, that this might have something to do with the original needle designs.

The tip modifications were made to three different types of original needles. The difference in these types was in the upper parts that are guiding the needle inside the nozzle. The original tip geometries were similar in all these types.

8.3 Diametral compression method

8.3.1 Un-notched nozzles

Typical results from diametral compression of un-used and used type A nozzles without a notch are shown in Figure 43. In every test, the crack initiated from the open end and proceeded towards the tip. After the first cracking sound, it was observed that the first crack had formed from the open end and reached approximately halfway of the sample length. When the load was still increased, it finally led to total breakage of the nozzle. The resulting cross-sections were always different, and only a fraction of the holes were fully visible from the whole length.

Figure 43. Un-notched type A nozzles after compression.

Behaviour of the un-notched type B nozzle was similar to type A nozzles. Resulted cross-sections can be seen in Figure 44.

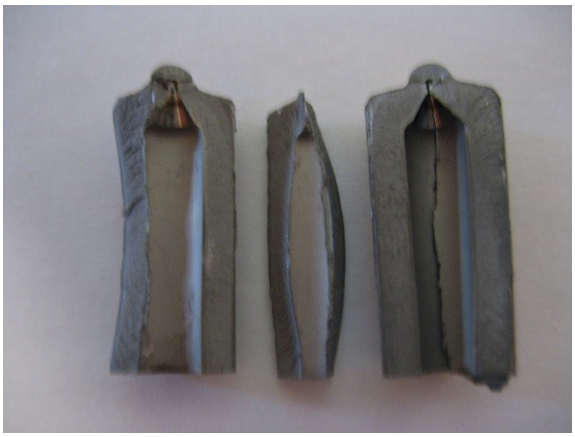

Figure 44. Un-notched type B nozzle after compression.

The test data revealed that the initial crack formed when the load was approximately between 20–25 kN. The final breakage happened usually between 25–30 kN. In general, unused nozzles fractured slightly earlier than used ones. Differences between individual nozzles also caused variations in the needed loads. The speed of loading did not seem to affect the type of fractures in any particular way.

8.3.2 Notched nozzles

The notched type A nozzles gave different results compared to un-notched type A nozzles. The results are shown in Figure 45. The notch in the un-used nozzle was not as deep as in the used one, which might be one reason for the different geometries.

The used nozzle was frozen and compressed manually. After the first cracking sound it was observed that the tip was detached from the nozzle and the rest of the nozzle remained un-cracked.

The un-used nozzle instead, was compressed with the compression test machine without the help of liquid nitrogen. As a result, half of the tip detached from the nozzle, but at the same time the rest of the nozzle broke to many longitudinal cross-sections like in the previous tests with un-notched type A nozzles.

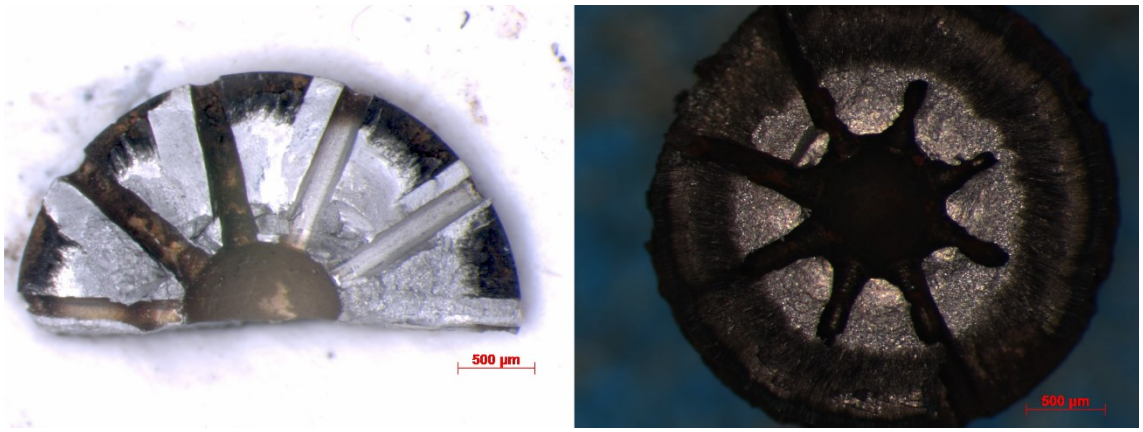

Figure 45. Notched type A nozzles after compression. Un-used nozzle on the left, used on the right.

The result achieved with the notched type B nozzle is presented in Figure 46. The result showed that the notches did not help in detaching only the tip from the nozzle. Instead, the achieved cross-sections resembled the ones that were achieved with an un-notched type B nozzle.

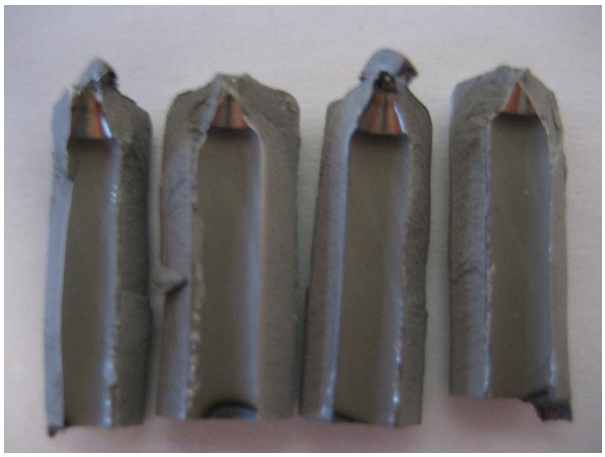

Figure 46. Notched type B nozzle after compression.

8.4 Silicone molding method

SEM was used to examine the surfaces of the two molds. The results showed that the silicone replica copied the surface reasonably well and different surface qualities could clearly be seen. When a mold of the un-used nozzle was compared to a mold of a used nozzle with deposits, an obvious difference could be seen between the surfaces. The pictures indicate that a layer of foreign particles has formed on the internal surfaces of the used nozzle.

However, it is impossible to identify where the fuel deposits are located. The layer is clearly more un-even, but the uniformity and the small size of the replicated particle shapes made it difficult to analyze by using SEM. Figure 47 illustrates the difference between the two molds.

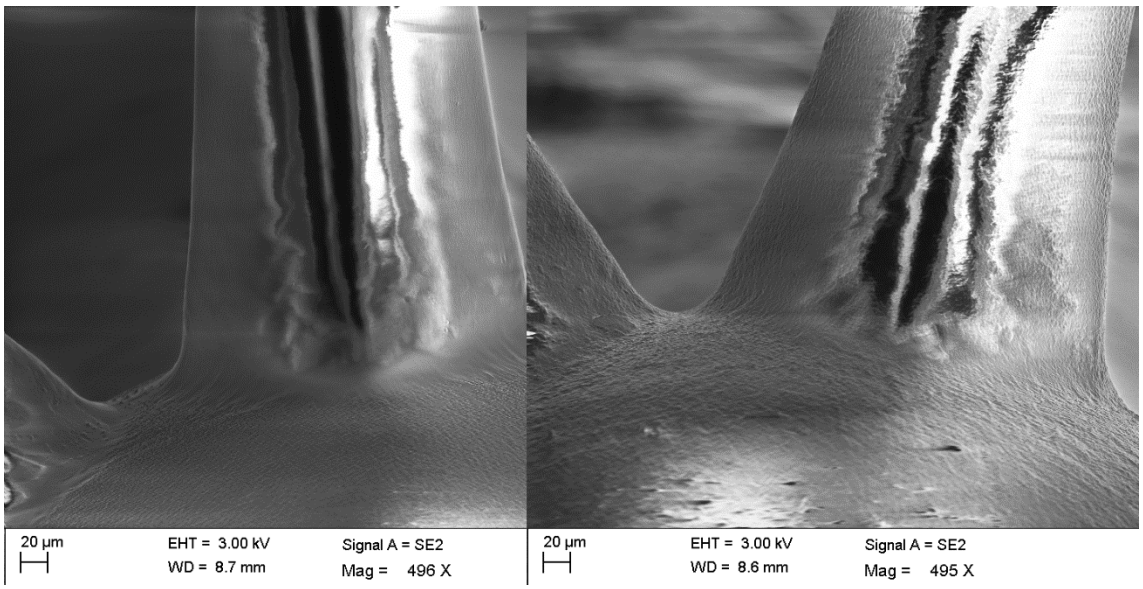

Figure 47. SEM pictures taken from the molds. Mold from the un-used nozzle on the left, mold from the used nozzle on the right.

A second mold was made from the used nozzle to test if the molding process removes particles from the surface. Images from the mold show that the fine layer is not affected. In addition to this, some clusters of bigger particles that were not present in the first mold, can be seen (Figure 48). The width of these particles varies from 2 to 25 µm. The particles have clearly attached to the mold from the nozzle surface. Since these particles were not present in the first mold, it was concluded that they might have attached to the nozzle surface during the first molding process. Another possibility is that these particles are fuel deposits.

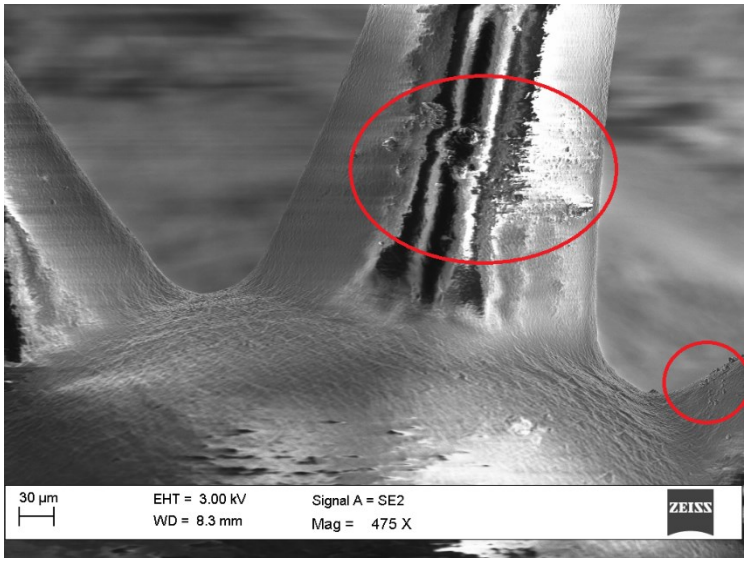

Figure 48. SEM picture from the second mold, made from the used nozzle.

9 Discussion

Best results were achieved with the drop-weight method. When the method was used for type A nozzles, the desired conical tip cross-section was achieved repeatedly and in most of them all the spray-holes were visible in full length. In a few samples, one or two holes had limited visibility, but only from a very short length. The same conical tip cross-section was achieved with type B nozzles, but the amount of revealed holes was not as regular and large as with type A nozzles. The reliability of the drop-weight testing method was high because the weight was guided to hit the same position every time and the nozzle position was highly constrained.

A great advantage is, that the same drop-weight method can be used for type A and type B nozzles to enable the microscopic examination of the spray-holes. With both nozzle types, the process is exactly the same and the same needle type can be used. The method does not include liquids or external heat sources, which could flush away or contaminate the fuel deposits. Only required preparations are the modifying of the needle tips and cutting the needles shorter. A disadvantage is, that the same needle can be only used for a limited amount of nozzles according to the performed tests. In addition, the needles can get stuck inside the nozzle. Both of these factors increase material losses. If a needle could be used a larger number of times, these material losses would decrease. A harder needle material could help to decrease the deformation rate.

The notching of a type A nozzle tip did not provide any additional benefit in the drop-weight method, except the reduced dropping height. The same result was achieved without a notch. The notch-effect was not tested with type B nozzles, which is something that could be done in the future to study if more preferable and repeatable results could be obtained.

The diametral compression method provided variable results. The results were always different when un-notched type A and type B nozzles were destroyed. The amount of revealed holes was irregular and the nozzles were fractured to different amount of pieces with inconsistent shape. The same problem appeared when a notched type B nozzle was destroyed. Notched type A nozzles provided more promising results under diametral compression. The nozzle that was compressed manually, proved that when the notch is deep enough, a conical tip cross-section can be obtained. The needed minimum depth of the notch should be defined if this method is to be used in the future. The manual placement of the nozzles causes uncertainty in the diametral compression method, because the position of the holes and the alignment of the nozzle was not constrained.

Laser cutting tests showed, that a narrow cut, which is applicable for injector nozzle sectioning, can be obtained. When a suitable combination of parameters was used, a compromise between the groove width and the processing time was found. Thermal effects during the process were observed to be minimal, which means the deposits should not be harmed if the laser beam is not allowed to be in direct contact with the walls of the spray-holes. In other words it means that the laser beam must be turned off every time it is crossing a hole and the cutting process has to be stopped before the beam enters through the material thickness inside the nozzle.

Due to the safety gap between the holes and the grooves, and the fact that the cutting cannot be performed entirely through the material, the laser method can only be used for notching the nozzle tip. The final breaking has to be done by using a different method. If the laser cutting method is to be used in the future, the number of passes before the beam enters inside the nozzle has to be determined for the used parameters.

The silicone molding method did not produce the wanted end result. The surface structure was different in a mold that was made from a used nozzle with deposits. Despite this, it was impossible to tell where the actual fuel deposit particles were located.

Based on the test results and conclusions, the best method for injector nozzle sectioning is the drop-weight method due to the simplicity, repeatability and the accessibility to the spray-holes it provides.

10 Conclusion

The objective of this master's thesis was to develop methods for injector nozzle sectioning. First target was to identify as many suitable methods as possible and choose the most potential ones for further examination. Second target was to study and test the suitability of the chosen methods in practice. Final target of the thesis was to develop a reliable and repeatable process for injector nozzle sectioning without contaminating or removing the fuel deposits inside the nozzle spray-holes.

All the targets of the thesis were obtained. Several potential methods were identified and the selected ones were tested. Based on the test results, a repeatable and reliable method for injector nozzle sectioning, called the drop-weight method, was developed. The method will be later used for studying of internal fuel deposits that are built up in the nozzle spray-holes.

References

1. Engine & emission technology online. *Dieselnet.* [Online] [Cited: 21 3 2016.] https://www.dieselnet.com/.

2. Injector Deposits. *Dieselnet.* [Online] [Cited: 21 3 2016.] https://www.dieselnet.com/tech/engine_fi_nozzle_deposits.php.

3. *Coking Phenomena in Nozzle Orifices of DI-Diesel Engines.* Tang, Jens, et al. SAE Int. J. Fuels Lubr. Issue 1, s.l. : SAE International, 2009, Vol. 2, pp. 259-272.

4. Steen, William M and Mazumder, Jyotirmoy. *Laser Material Processing, Fourth Edition.* s.l. : Springer, 2010.

5. Davim, J. Paulo. *Nontraditional machining processes.* s.l. : Springer, 2013.

6. *Laser beam machining—A review.* Dubey, Avanish Kumar and Yadava, Vinod. International Journal of Machine Tools & Manufacture 48, s.l. : Elsevier Ltd., 2007, pp. 609–628.

7. *Energy and Resource Efficiency of Laser Cutting Processes.* Kellens, Karel, et al. Physics Procedia 56, s.l. : Elsevier B.V, 2014, pp. 854 – 864.

8. PennWell Corporation. High power beam analysis. *Industrial Laser Solutions.* [Online] [Cited: 24 3 2016.] http://www.industrial-lasers.com/articles/print/volume-28/issue-5/features/high-power-beam-analysis.html.

9. *Investigation of micro-milling process parameters for surface roughness and milling depth.* Saklakoglu, Ibrahim Etem and Kasman, Sefika. s.l. : Springer-Verlag London Limited, 2010.

10. Koc, Muammer and Özel, Tugrul. *MICRO-MANUFACTURING, Design and manufacturing of micro-products.* s.l. : John Wiley & Sons, Inc, 2011.

11. *Micro-machining with ultrashort laser pulses: From basic understanding to technical applications.* Dausinger, Friedrich, Hugel, Helmut and Konov, Vitali.

12. *High-precision helical cutting using ultra-short laser pulses.* He, Chao, et al. Physics Procedia 56, s.l. : Elsevier B.V., 2014, pp. 1066-1072.

13. Callen, James D. *Fundamentals of Plasma Physics.* s.l. : J.D Callen, 2003.

14. *Investigation Analysis of Plasma arc cutting Parameters on the Uneveness surface of Hardox-400 material.* Chamarthi, Subbarao, et al. Procedia Engineering 64, s.l. : Elsevier Ltd., 2013, pp. 854 – 861.

15. *Experimental study of the features of the kerf generated by a 200 A high tolerance plasma arc cutting system.* Bini, R., et al. Journal of Materials Processing Technology 196, s.l. : Elsevier B.V., 2007, pp. 345-355.

16. *Comparison Metal Water Jet Cutting with Laser and Plasma Cutting.* Krajcarz, Daniel. Procedia Engineering 69, s.l. : Elsevier Ltd., 2014, pp. 838-843.

17. *Experimental Investigation of the Plasma Arc Cutting Process.* Salonitis, K. and Vatousinanos, S. Procedia CIRP 3, s.l. : Elsevier B.V., 2012, pp. 287-292.

18. The Welding Institute. Cutting processes - plasma arc cutting - process and equipment considerations. [Online] [Cited: 4 11 2015.] http://www.twi-global.com/technical-knowledge/job-knowledge/cutting-processes-plasma-arc-cutting-process-and-equipment-considerations-051/.

19. *The Principle of Plasma Cutting Technology and Six Fold Plasma Cutting.* Hatala, Michal. 5th International Multidisciplinary Conference.

20. Axis International Inc. Plasma vs Laser cutting: Weighing the options. [Online] [Cited: 4 11 2015.] http://www.axisplasma.com/documents/plasma_vs_laser_cutting_weighing_the_options.pdf.

21. Icon Machine Tool, Inc. Laser vs. Plasma. [Online] 10 2008. [Cited: 4 11 2015.] http://www.iconmachinetool.com/education/Laser%20vs%20Plasma.pdf.

22. ESAB. Plasma Solutions-Micro Nozzle Technology. [Online] [Cited: 10 11 2015.] http://www.esabna.com/us/en/mechanized/process_solutions/plasma_solutions/plasma_consumables/micro-nozzle-technology.cfm.

23. *Ion beam, focused ion beam, and plasma discharge machining.* Allen, D.M., et al. CIRP Annals - Manufacturing Technology 58, s.l. : CIRP, 2009, pp. 647-662.

24. E.A. Fischione Instruments, Inc. Microelectronic device delayering using an adjustable broad-beam ion source. [Online] 2013. [Cited: 15 11 2015.] http://www.fischione.com/uploads/pdfs/application-pdfs/AN004.pdf.

25. Top Analytica Ltd. Broad Ion Beam Cross Sectioning. [Online] [Cited: 15 11 2011.] http://www.topanalytica.com/files/160/Broad_Ion_Beam_Cross_Sectioning.pdf.

26. *A Review of Focused Ion Beam Sputtering.* Ali, Mohammad Yeakub, Hung, Wayne and Yongqi, Fu. INTERNATIONAL JOURNAL OF PRECISION ENGINEERING AND MANUFACTURING Vol. 11, s.l. : Springer, 2010, pp. 157-170.

27. Ishitani, Tohru, Ohnishi, Tsuyoshi and Yagushi, Toshie. Chapter 13, Focused Ion Beams and interaction with solids. [book auth.] A Tseng Ampere. *Nanofabrication-Fundamentals and Applications.* s.l. : World Scientific Publishing Co. Pte. Ltd., 2008.

28. *Recent developments in micromilling using focused ion beam technology.* Ampere, A Tseng. Journal of Micromechanics and Microengineering 14, s.l. : Institute of Physics Publishing, 2004, pp. 15-34.

29. *Applications of focused ion beam SIMS in materials science.* McPhail, David S., Chater, Richard J. and Li, Libing. Microchim Acta 161, s.l. : Springer-Verlag, 2008, pp. 387-397.

30. *Plasma FIB: Enlarge your field of view and your field of applications.* Garnier, A., et al. Microelectronics Reliability 55, s.l. : Elsevier Ltd., 2015, pp. 2135-2141.

31. *Combined plasma FIB-SEM.* Hrncir, T., et al. MICROSCOPY AND MICROANALYSIS 18, 2012, pp. 652-653.

32. *High speed micro-fabrication using inductively coupled plasma ion source based focused ion beam system.* Menon, Ranjini and Nabhiraj, P.Y. Vacuum 111, s.l. : Elsevier Ltd, 2014, pp. 166-169.

33. Hrncir, T., et al. Novel plasma FIB/SEM for high speed failure analysis, 3D tomography and other applications. [Online] [Cited: 16 11 2015.] http://www.emc2012.org.uk//documents/Abstracts/Abstracts/EMC2012_0902.pdf.

34. Engineering, The International Academy for Production. *CIRP Encyclopedia of Production Engineering.* s.l. : CIRP, 2014. pp. 446-452.

35. El-Hofy, Hassan. *Advanced Machining processes, Nontraditional and Hybrid Machining Processes.* s.l. : McGraw-Hill, 2005.

36. Singh, Rajender. *Introduction to basic manufacturing processes and workshop technology.* s.l. : New Age International Publishers, 2006.

37. Hurco Companies, Inc. Why NuCon Chose Hurco VMX42SR 5-Axis Machining Centers. [Online] 2012. [Cited: 8 3 2016.] http://www.hurco.com/in/why-hurco/success-stories/blog/default.aspx.

38. Davim, J. Paulo. *Modern Mechanical Engineering, Materials Forming, Machining and Tribology.* s.l. : Springer-Verlag, 2014. pp. 325-365.

39. *Command Shaping Control for Micro-milling Operations.* Fortgang, Joel, et al. International Journal of Control, Automation, and Systems 9, s.l. : Springer, 2011, pp. 1136-1145.

40. *Cutting force model considering tool edge geometry for micro end milling process.* Journal of Mechanical Science and Technology 22, s.l. : Springer, 2008, pp. 293-299.
41. *Influence of tool wear on machining forces and tool deflections during micro milling.* Oliaei, Samad Nadimi Bavil and Karpat, Yigit. The International Journal of Advanced Manufacturing Technology, s.l. : Springer-Verlag, 2015, pp. 1-18.

42. Performance Micro Tool. Nano Tools. [Online] [Cited: 20 11 2015.] http://www.pmtnow.com/nano.

43. Society of Manufacturing Engineers. Basics of Grinding. [Online] [Cited: 9 11 2015.] http://manufacturing.stanford.edu/processes/Grinding.pdf.

44. *Novel Grinding Tools for Machining Precision Micro Parts of Hard and Brittle Materials.* Hoffmeister, H.W. and Wenda, Andreas. Proceedings of 15th Annual Meeting of the ASPE, Scottsdale, Arizona : s.n., 2000, pp. 152-155.

45. *Ultra-precision grinding.* Brinksmeier, E., et al. s.l. : Elsevier, 2010, Vols. CIRP Annals - Manufacturing Technology 59, pp. 652-671.

46. *Development of a Dicing Blade with Photopolymerizable Resins for Improving Machinability.* Lee, S.B., Enomoto, Tani Y. and Sato, H. CIRP Annals - Manufacturing Technology 54, pp. 293-296.

47. *Micro grinding tool for manufacture of complex structures in brittle materials.* Aurich, J.C., et al. CIRP Annals - Manufacturing Technology 58, 2009, pp. 311-314.

48. *Grinding of Microstructures in Hardened Steel with CBN Tools.* Hoffmeister, H.W. and Hlavac, M. Proceedings of the 17th Annual Meeting of the ASPE, vol 27, St. Louis, USA : s.n., 2002, pp. 490-494.

49. Sandvik Coromant. Metalcutting Technical Guide (A) General Turning. [Online] [Cited: 20 11 2015.] http://www2.coromant.sandvik.com/coromant/pdf/Metalworking_Products_061/tech_a_1.pdf.

50. *Methods to Improve Production Rate in Turning Operation.* Patokar, Pradeep, et al. International Journal of Research in Advent Technology, Vol.2, No.3, 2014, pp. 329-334.

51. Kalpakijan and Schmid. *Manufacturing Processes for Engineering Materials, 5th ed.* s.l. : Pearson Education, 2008.

52. Cheng, Kai and Dehong, Huo. *Micro-Cutting : Fundamentals and Applications.* s.l. : John Wiley & Sons, 2013.

53. *Micro-turning of hard steel by single-grain ceramic cutter based on numerical simulations.* Huang, W.J. and Hu, H.J. Ceramics International 40, s.l. : Elsevier Ltd., 2014, pp. 13057-13065.

54. Prof. Kailas, Satish V. Materials Science. *Scribd.* [Online] [Cited: 26 11 2015.] http://www.scribd.com/doc/77101399/Material-Science#scribd.

55. Maleque, M.A. and Salit, M.S. *Materials Selection and Design, Chapter 2: Mechanical Failure of Materials.* s.l. : Springer, 2013.

56. Milella , Pietro Paolo. *Fatigue and Corrosion in Metals.* 2013 : Springer.

57. Kokcharov, Igor. Structural Integrity Analysis: Stress Concentration. [Online] [Cited: 26 11 2015.] http://www.kokch.kts.ru/me/t1/SIA_1_Stress_Concentration.pdf.

58. Francois, Dominique, Pineau, Andre and Zaoui, Andre. *Mechanical Behaviour of Materials, Volume II: Fracture Mechanics and Damage.* s.l. : Springer, 2013.

59. SP Technical Research Institute of Sweden. *Materials testing of metals.* [Online] [Cited: 27 11 2015.] http://www.sp.se/en/index/services/materialstestingofmetals/sidor/default.aspx.

60. The Nuffield Foundation. *Impact testing* . [Online] 2008. [Cited: 27 11 2015.] http://www.nuffieldfoundation.org/sites/default/files/09_Impact_testing.pdf.

61. Steinwall Inc. Plastic Data Sheets Explanation, Impact testing. [Online] [Cited: 27 11 2015.] http://www.steinwall.com/pages/ImpactTesting.

62. pixhder.com Inc. Impact Fracture Testing. [Online] [Cited: 21 3 2016.] http://pixhder.com/impacted+fracture+diagram?image=488208271.

63. Univer Technologies Group. ASTM D2444 Standard Test Method for Determination of the Impact Resistance of Thermoplastic Pipe and Fittings by Means of a Tup (Falling Weight). [Online] [Cited: 27 11 2015.] http://www.univer-test.com/en/sol-detail.asp?id=177.

64. MATERIALS EVALUATION AND ENGINEERING INC. Tension and Compression Testing. [Online] [Cited: 27 11 2015.] http://www.mee-inc.com/hamm/tension-and-compression-testing/

65. *Introduction to Tensile Testing.* ASM International. Tensile Testing, Second Edition (#05106G), 2004.

66. *Mechanical and Thermal Properties of Ceramics.* Wachtman Jr., J.B. Mechanical and Thermal Properties of Ceramics: Proceedings, Issue 303, s.l. : United States National Bureau of Standards, 1969, pp. 249-256.

67. Quizlet Inc. Property of materials. [Online] [Cited: 14 12 2015.] https://quizlet.com/4157499/property-of-materials-flash-cards/.

68. *NEW TECHNIQUE FOR DETERMINATION OF INTERNAL GEOMETRY OF A DIESEL NOZZLE WITH THE USE OF SILICONE METHODOLOGY.* Macian , V., et al. Experimental Techniques 2, 2003, Vol. 27, pp. 39-46.

69. Marghitu, Dan B. *Mechanical Engineer's Handbook, Chapter 3 : Mechanics of Materials.* s.l. : ACADEMIC PRESS, 2001.

70. *Impact and Drop Testing with ICP Force Sensors.* Metz, Robert. SOUND AND VIBRATION MAGAZINE / FEBRUARY 2007, pp. 18-20.

71. Mäkelä, Mikko, et al. *Tekniikan Kaavasto.* s.l. : Tammertekniikka, 2010.

72. *Measurement of Indirect Tensile Strength of Anisotropic Rocks by the Ring Test.* Chen, C.S. and Hsu, S.C. Rock Mechanics and Rock Engineering 34, s.l. : Springer-Verlag, 2001, pp. 293-321.

73. Sahoo, Prasanta. *Engineering Tribology, Chapter 3: Surface Contact.* s.l. : PHI Learning Private Ltd., 2011.

74. Struers. *RepliSet Reference Guide, Manual NO.: 50900044.* 2011.

75. *Developments in the non-traditional machining of particle reinforced metal matrix composites.* Pramanik, A. International Journal of Machine Tools & Manufacture 86, s.l. : Elsevier Ltd., 2014, pp. 44-61.

Appendices

Appendix 1. Technical drawing of the laser holder. 1 page.
Appendix 2. Technical drawings of modified needle tips. 3 pages.

Appendix 1. Technical drawing of the laser holder

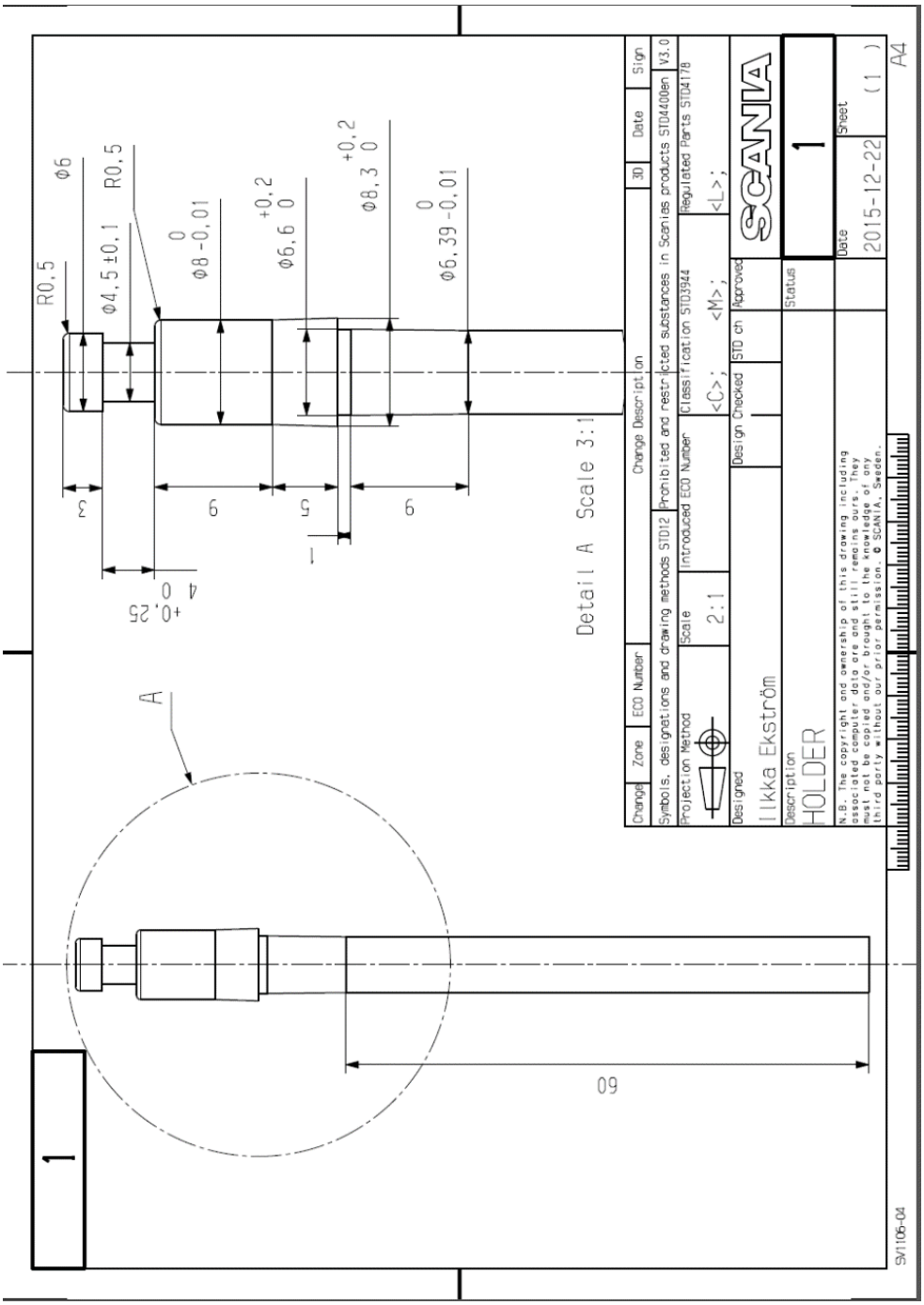

Appendix 2. Technical drawings of modified needle tips

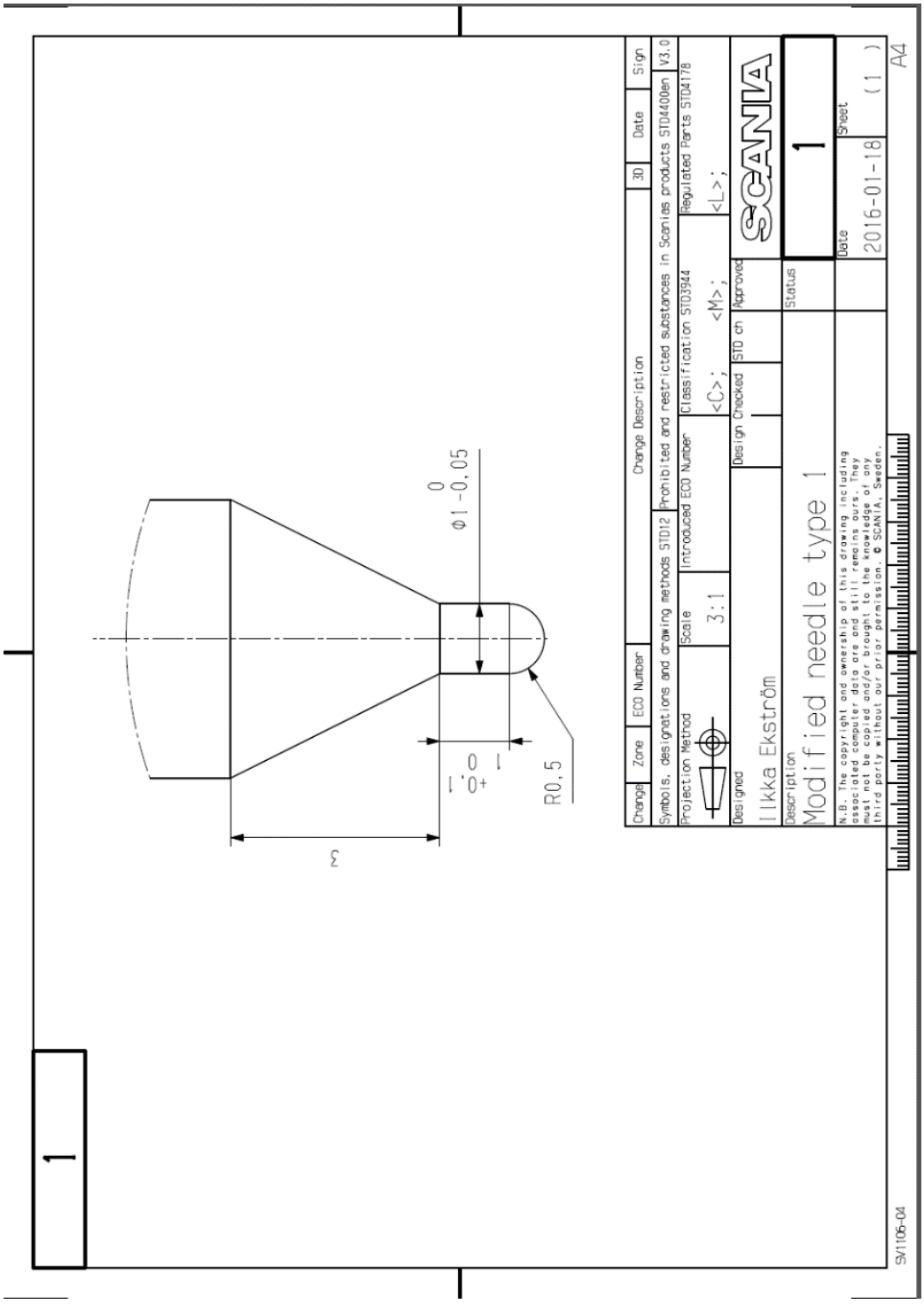

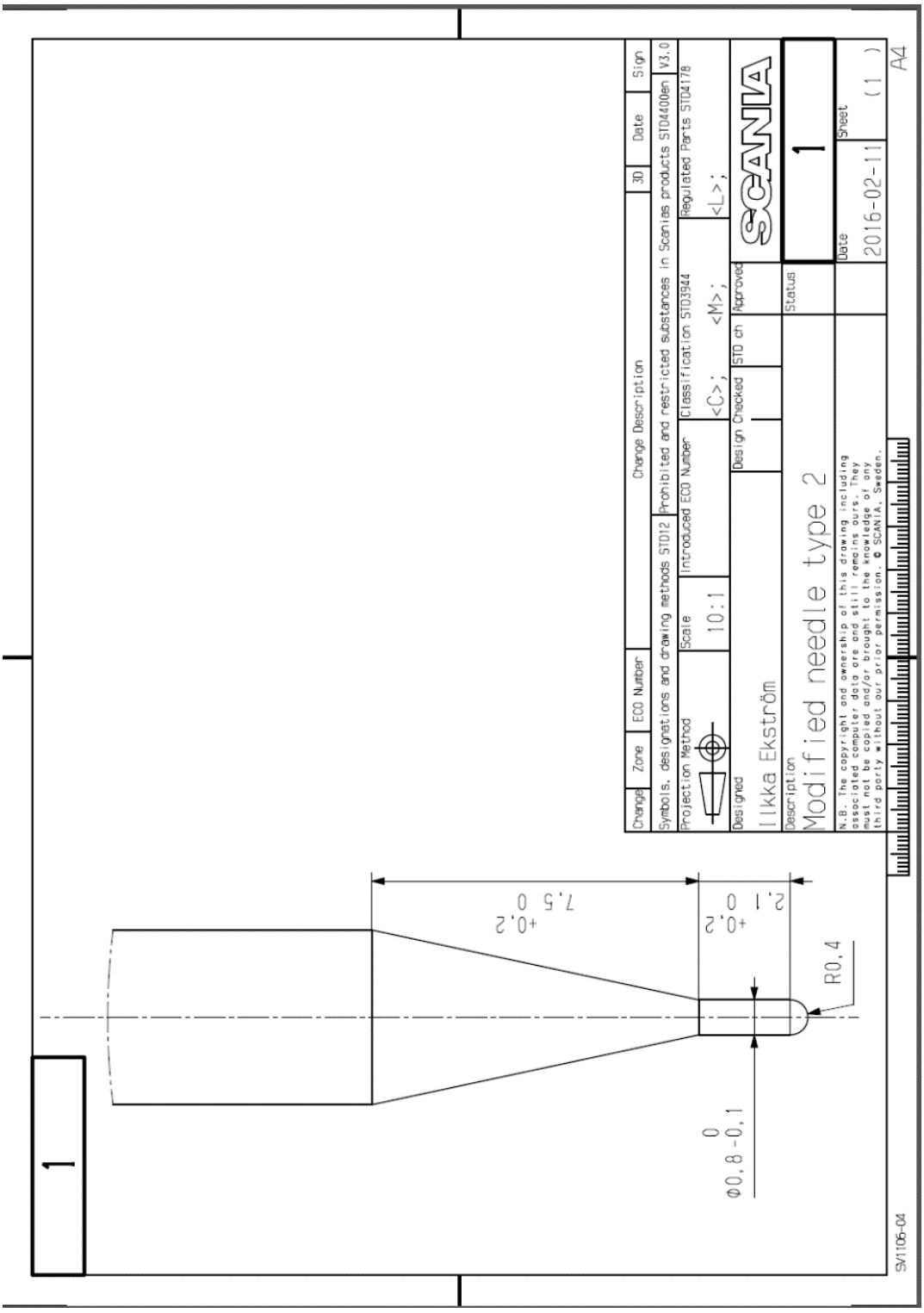
Change
Zone
ECO Number
Change Description
3D
Date
Sign
Symbols, designations and drawing methods STD12
Prohibited and restricted substances in Scanias products STD4400en V3.0
Projection Method
Scale
10:1
Introduced ECO Number
Classification STD3944
<C>; <M>;
Regulated Parts STD4178
<L>;
Designed
Ilkka Ekström
Design Checked
STD ch
Approved
SCANIA
Description
Modified needle type 2
Status
1
Date
2016-02-11
Sheet
(1)
A4
N.B. The copyright and ownership of this drawing including associated computer data are and still remains ours. They must not be copied and/or brought to the knowledge of any third party without our prior permission. © SCANIA, Sweden.
SV1106-04
1
7,5 0 +0,2
2,1 0 +0,2
R0,4
Φ0,8 0 -0,1

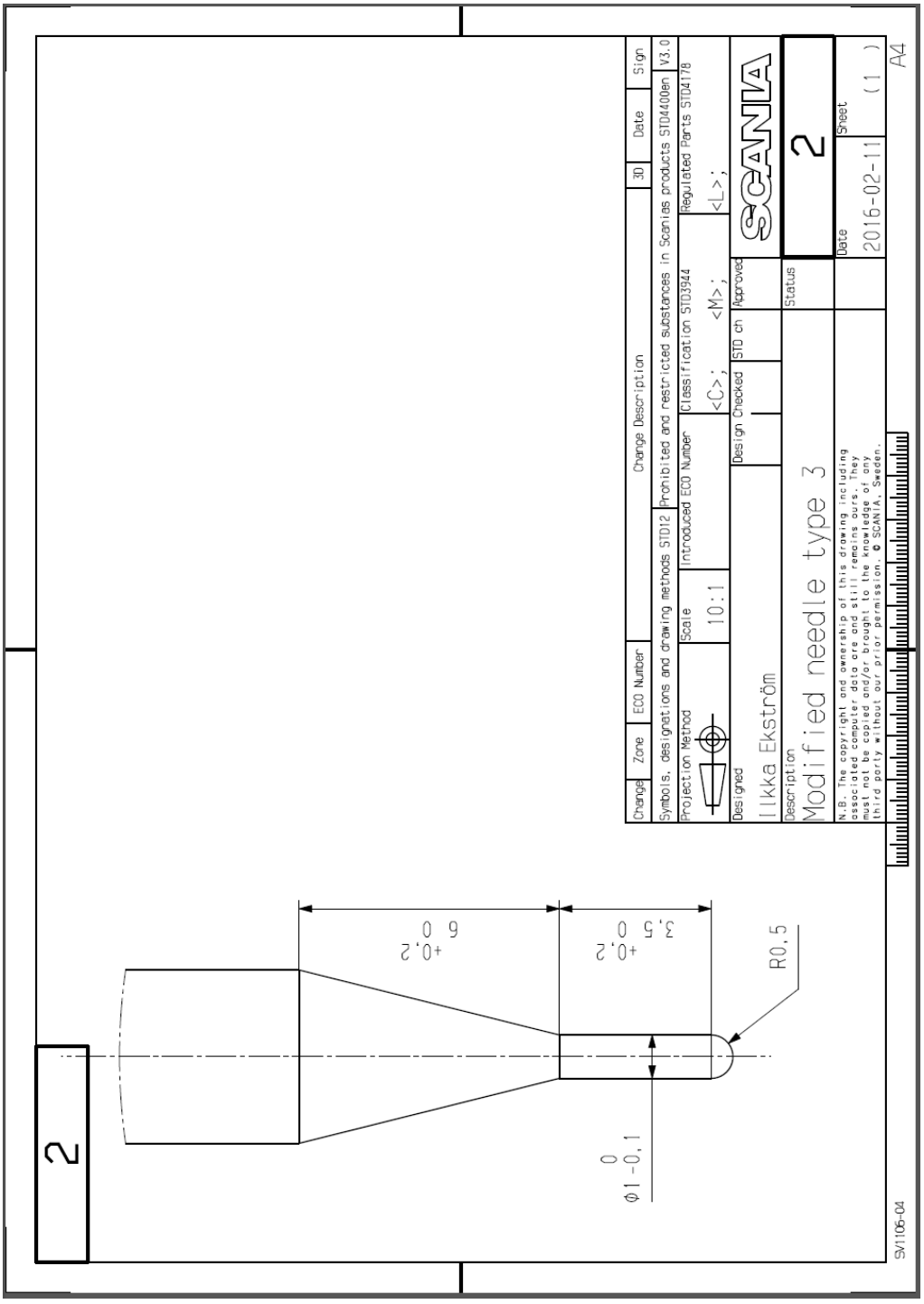
Change
Zone
ECO Number
Change Description
3D
Date
Sign
Symbols, designations and drawing methods STD12
Prohibited and restricted substances in Scanias products STD4400en
V3.0
Projection Method
Scale
10:1
Introduced ECO Number
Classification STD3944
<C>;
<M>;
Regulated Parts STD4178
<L>;
Designed
Ilkka Ekström
Design Checked
STD ch
Approved
SCANIA
Description
Modified needle type 3
Status
2
Date
2016-02-11
Sheet
(1)
A4
N.B. The copyright and ownership of this drawing including associated computer data are and still remains ours. They must not be copied and/or brought to the knowledge of any third party without our prior permission. © SCANIA, Sweden.
SV1105-04
2
R0,5
ϕ1 -0,1
0
3,5 +0,2
0
6 +0,2
0